Reliability Engineering and System Safety 242 (2024) 109789

Contents lists available at ScienceDirect

Reliability Engineering and System Safety

journal homepage: www.elsevier.com/locate/ress

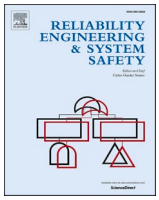

Methodology for probabilistic tsunami-triggered oil spill fire hazard assessment based on Natech cascading disaster modeling

Tomoaki Nishino [a,*], Takuya Miyashita [a], Nobuhito Mori [a,b]

[a] Disaster Prevention Research Institute, Kyoto University, Gokasho, Uji, Kyoto 611-0011, Japan
[b] School of Engineering, Swansea University, Bay Campus, Fabian Way, Crymlyn Burrows, Skewen, Swansea SA1 8EN, UK

ARTICLE INFO

Keywords:
Natech
Emerging risk
Tsunami fire
Oil spill fire
Probabilistic tsunami hazard analysis (PTHA)
Uncertainty

ABSTRACT

A novel modeling methodology is presented for cascading disasters triggered by tsunami hazards considering uncertainties. The proposed methodology focuses on tsunami-triggered oil spills and subsequent fires, a type of natural hazard-triggered technological (Natech) event. The methodology numerically simulates the time-varying behavior of tsunami-triggered oil spill fires for numerous stochastically generated scenarios and performs a probabilistic mapping of the maximum radiative heat flux as a quantitative measure of the fire hazard. To enable these assessments, probabilistic tsunami hazard assessments are extended to include the tsunami-induced movement of oil storage tanks, resulting oil spills, tsunami-driven oil fire spread, and thermal radiation from fires. The uncertainty of the earthquake fault slip distribution, oil filling level of storage tanks, and fire starting time and position is incorporated into the new assessments. To demonstrate the methodology, a realistic case study is conducted for a coastal petrochemical industrial park in Japan conditioned on possible offshore moment magnitude 9.1 earthquakes. Contrary to typical tsunami direct impact assessments, the results highlight the cascading effects of tsunamis and large variability in key output variables concerning oil spills and fires. This indicates that the methodology is useful for deepening stakeholders' understanding of tsunami-triggered cascading disasters and improving risk reduction plans.

1. Introduction

The emerging tsunami fire hazard [1] was highlighted by the 2011 Tohoku earthquake, which occurred off the Pacific coast of Tohoku, Japan, on March 11, 2011 (14:46 local time) with a moment magnitude (Mw) of 9.0. The 2011 Tohoku earthquake caused a massive tsunami that struck an approximately 2000-km stretch along the Pacific coast of Japan and inundated over 400 km^2 of land [2]. The tsunami washed away houses, bridges, and other various items from land; hazardous material spills were caused by damaged liquefied petroleum gas cylinders for household use, automobiles, and oil storage tanks, resulting in the occurrence of 124 fire ignitions in inundated areas [1]. Some of these tsunami fires spread to nearby floating or accumulated combustible materials, either torn from houses by the tsunami or constituting the wooden houses themselves, and eventually developed into conflagrations involving over 61 ha of land [1,3]. This exceeds the 46 ha destroyed by fires following the 1995 Kobe earthquake; such conventional post-earthquake fires (i.e., fires caused by ground shaking) are seriously considered in earthquake-prone countries worldwide [e.g., 4, 6,10,13].

Of the tsunami fires following the 2011 Tohoku earthquake, the oil spill fire in Kesennuma Bay, Miyagi, Japan, was the most notable, causing devastating damage to coastal communities and environments [14]. Fig. 1 shows several images reflecting the actual situation of the fire. The tsunami, with a height of up to 6 m, washed away 22 oil storage tanks in the port of Kesennuma that stored fuel used for fishing ships, resulting in 11521 kL of oil spills, mostly fuel oil as specified by Japanese Industrial Standards (having properties close to those of diesel oil) [15]. The tsunami spread the oil throughout the bay; the oil was then ignited in the bay even though the flash point is much higher than ordinary temperatures. Fire experiments [16] suggest that burning floating debris, such as wooden material, was a potential ignition source and may have ignited the floating oil, acting as a candle wick. The fire spread rapidly over the floating oil and eventually transformed the bay into a sea of flames. An analysis of image records [14] indicates that the fire front moved at velocities of over 1.6 m/s, approximately a hundredfold faster than the flame spread rate over non-gasoline-type oil floating on static water at ordinary temperatures [17–19]. A numerical analysis

* Corresponding author.
E-mail address: nishino.tomoaki.3c@kyoto-u.ac.jp (T. Nishino).

https://doi.org/10.1016/j.ress.2023.109789
Received 19 January 2023; Received in revised form 2 October 2023; Accepted 2 November 2023
Available online 4 November 2023

[14] suggests that the transport of burning oil by the tsunami greatly contributed to the fire development; that is, it was a tsunami-driven oil fire. The fire led to various secondary fires, e.g., building, ship, and forest fires, resulting in approximately 247 ha of burned areas including outside the inundation areas [14]. Notably, the fire affected tsunami vertical evacuation buildings, which are known to be effective risk reduction measures for coastal communities without accessible high ground. Consequently, people who had escaped into these buildings from the tsunami encountered fire dangers [20].

These tsunami fire experiences highlight an important aspect of coastal area safety, particularly in areas with installations storing or handling petroleum products. Historically, tsunamis have struck coastal industrial zones and triggered oil spill fires following large offshore earthquakes, e.g., the 1964 Alaska [21] and 1964 Niigata [22] earthquakes. Therefore, tsunami-triggered oil spill fires are a universal potential hazard that many tsunami-prone countries face. However, typical tsunami risk management has focused on the direct impact of tsunamis on humans and assets and has not considered the impact of fires as a secondary tsunami hazard. Therefore, improving tsunami risk management is an important task for coastal stakeholders. This requires a methodology for quantitatively evaluating tsunami-triggered oil spill fire hazards.

Tsunami-triggered oil spill fires are a type of Natech event, that is, a technological disaster triggered by natural hazards [23], the incidence of which has significantly increased in recent decades [24]. Natech events result from the impact of natural hazards on industrial installations storing or handling hazardous substances and can include severe accidents, such as substance releases, triggered fires, and explosions, as a consequence of equipment damage. Because improving Natech risk management is increasingly recognized as a priority, many studies have focused on equipment fragility assessments and Natech hazard or risk assessments for several types of natural hazards, including earthquakes [e.g., 25–28], floods [e.g., 29–33], and lightning [e.g., 34–36], which typically have addressed cascading disasters triggered by domino effects [e.g., 5,7,8] and the performance of safety barriers aimed at preventing domino effects [e.g., 9,11,12]. However, few studies have addressed tsunamis in the context of Natech risk management. Consequently, methodologies for tsunami-related Natech hazard or risk assessments are not well established. However, several contributions have been made to understanding such events. These include analyses of the potential release of hazardous materials from tsunami damage to equipment based on numerical tsunami simulations for hypothetical scenarios [37], the tsunami impact on chemical industries following the 2011 Tohoku Earthquake [38], simplified modeling of the vulnerability of industrial storage tanks to tsunamis and transported debris [39], experimental investigations of tsunami wave loads acting on cylindrical storage tanks and validation of empirical equations [40], two-layer hydrodynamic modeling of oil spread on tsunami inundation flow [22], numerical analyses of tsunami-triggered oil spills from coastal industrial zones for a hypothetical offshore earthquake scenario [41], computationally efficient local probabilistic tsunami hazard assessments for a coastal oil refinery area [83], and qualitative assessments of the potential for fires following a hypothetical scenario tsunami in ports with petrochemical facilities [82].

The above studies on tsunami-related Natech events do not model subsequent fires, which can lead to further catastrophic consequences. Therefore, alone they cannot effectively improve risk management. Conversely, a pioneering study [14] has attempted to develop a model to numerically simulate the dynamic behavior of tsunami-triggered oil spill fires, and validated the model performance against the tsunami fire in Kesennuma Bay following the 2011 Tohoku earthquake by comparing the model prediction to the fire department survey report and image records of tsunami evacuees. Subsequently, the model was applied to a coastal petrochemical industrial park focusing on a specific offshore

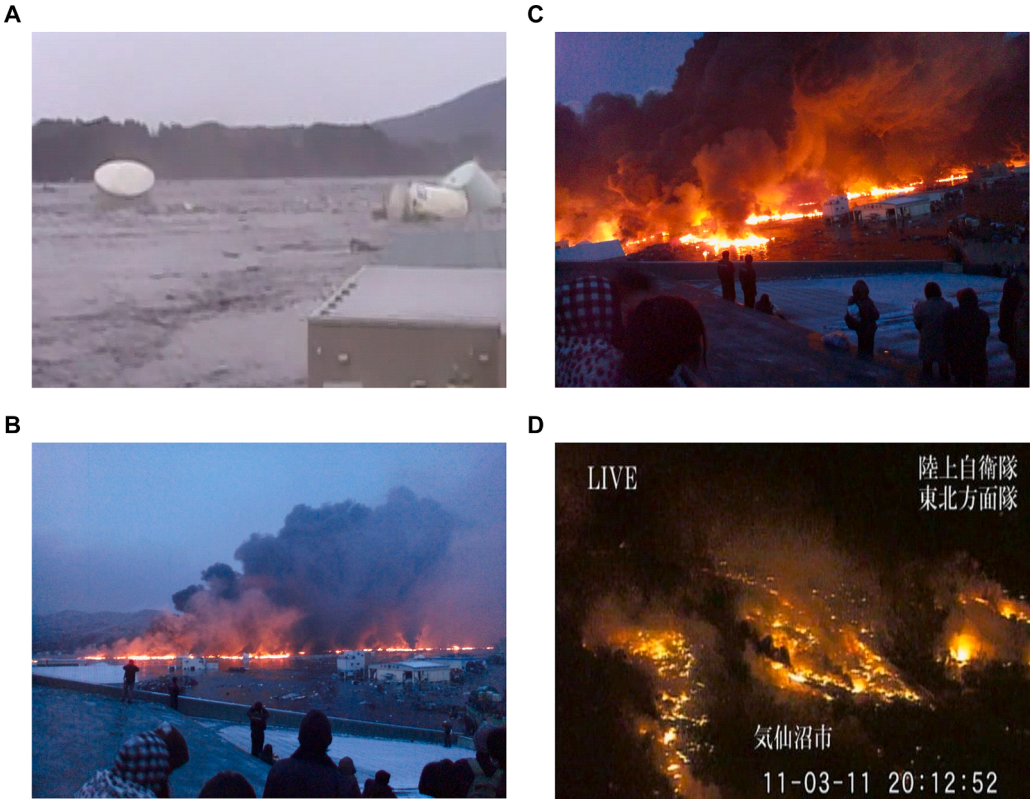

Figure 1. Tsunami-triggered oil spill fires in Kesennuma Bay, Miyagi, Japan, after the 2011 Tohoku earthquake: images taken by (A) the Japan Coast Guard around 3:30 p.m. on March 11, 2011; Ryosuke Onodera at (B) 5:53 p.m. and (C) 6:00 p.m. on March 11, 2011; and (D) the Japan Ground Self-Defense Force at 8:12 p.m. on March 11, 2011.

earthquake scenario [42]. The maximum radiative heat flux was mapped as a quantitative fire hazard measure to understand the potential horizontal extent of strong radiative heating. This fire hazard mapping enables the identification of potential consequences of fires, which is impossible in typical tsunami risk management.

Previous studies [14,42] presented a deterministic methodology for quantitative tsunami-triggered oil spill fire hazard assessments, limiting assessments to specific scenarios as opposed to providing probabilistic fire hazard information. Because the behavior of tsunami-triggered oil spill fire spreading greatly depends on the tsunami flow, tsunami variability, which primarily depends on the large uncertainty of earthquake fault rupture scenarios, could be an important factor affecting fire hazard assessments. Uncertainty in the constantly changing oil filling level of storage tanks can also affect fire hazard assessments via the probabilistic behavior of the tsunami-induced tank movement and resulting oil spills. Furthermore, uncertainty in when and where oil is initially ignited can significantly affect fire hazard assessments. Therefore, a probabilistic methodology comprehensively considering various uncertainties associated with fire hazard assessments is essential. Deterministic approaches that consider only a specific worst-case scenario may not provide realistic solutions. Conversely, probabilistic approaches could enable reasonable decision-making in Natech risk management.

Since 2000, probabilistic tsunami hazard assessments (PTHAs) have been well established [43,44,79,80]. PTHAs quantify the probability of exceeding specified levels of tsunami intensity measures (e.g., inundation depth and flow velocity) at a given location within a specified time period, and summarize this probabilistic information in hazard curves or hazard maps for use in engineering design, risk management, and evacuation planning. Logic trees are widely used to incorporate uncertainties into PTHAs, expressing not only the uncertainty of the key source parameters, but also the uncertainty due to numerical model selection or bathymetry/topography dataset bias, with weights assigned to their branches [e.g., 45–49]. On the other hand, random phase approaches have been used as alternative ways to consider source-related uncertainty (e.g., slip distribution, source location, magnitude, and etc.) as a statistical ensemble [e.g., 50–54]. The random phase approach is a kind of Monte Carlo simulation and stochastically generates numerous synthetic fault slip distributions with varying magnitudes based on seismological constraints by the scaling relationships of earthquake source parameters for subduction zones [52].

If PTHA frameworks can be extended to include tsunami-triggered oil spill fire analyses, this would enable unprecedented assessments of tsunami-related Natech hazards, deepening stakeholders' understanding of tsunami-triggered cascading disasters and promoting better tsunami risk management, including triggered fire risks. The random phase approach is suitable for this extension compared to the logic tree approach because tsunami-triggered cascading disaster analyses require a large ensemble that considers links between different physical process models. In this case, the source-related uncertainty, one of the largest uncertainties, is considered, although uncertainties due to numerical model selection and bathymetry/topography dataset bias are not considered.

This study develops a methodology for probabilistic tsunami-triggered oil spill fire hazard assessments (PTFHAs) as an extension of PTHAs. The methodological contribution of this study is the physics-based integrated modeling of a sequence of tsunami-related Natech cascading phenomena, including previously unconsidered tsunami fires, incorporating uncertainties to provide a probabilistic basis for enhancing safety planning for coastal areas with petrochemical facilities. The proposed methodology enables a probabilistic mapping of the maximum radiative heat flux as a quantitative measure of the fire hazard by focusing on uncertainties in the earthquake rupture process, oil filling condition of storage tanks, and initial oil ignition. These uncertainties are incorporated into the PTFHA via a series of numerical simulations of tsunami propagation and inundation, tsunami-induced movement of oil storage tanks and resulting oil spills, tsunami-driven oil fire spread, and thermal radiation from fires for numerous stochastically generated scenarios. The tsunami-induced tank movement and resulting oil spills are modeled for atmospheric storage tanks with fixed roofs storing liquids at ambient pressure. For simplicity, the PTFHA is conditioned on a specified earthquake magnitude. Namely, uncertainty in both the location and geometry of the fault plane and the slip distribution over the fault plane is considered under the specified magnitude, while the possible occurrence of earthquakes with different magnitudes is not considered. In this sense, the PTFHA in this study is not complete, but it can be extended to include the earthquake occurrence uncertainty using the Gutenberg–Richter law [56]. To demonstrate the methodology, a realistic case study is conducted for the Port of Osaka, Japan, which contains a petrochemical industrial park with over 200 oil storage tanks, focusing on possible offshore megathrust earthquakes. Essential points include (1) the variability in the key outputs concerning tsunamis, oil spills, and fires, (2) locations likely to be exposed to strong radiative heating, (3) particular characteristics of intense fire hazard locations and contributing factors, (4) important facilities, such as tsunami vertical evacuation structures, at high risk from fire hazards, and (5) recommended fire risk reduction measures. Explosions and other types of fires related to hazardous materials, such as tank fires and ship fires, are not considered in the assessments and are left to future work.

This paper is organized as follows. Section 2 defines the hazard equation for tsunami-triggered oil spill fires and presents the computational framework and implemented models. Section 3 describes the numerical setup to illustrate the PTFHA via the case study. Section 4 presents and discusses the key results of the case study. Finally, Section 5 presents the study conclusions and potential future work.

2. Proposed methodology

2.1. Fire hazard formulation

Tsunami-triggered oil spill fires are modeled as a sequence of the following events. (1) A tsunami is generated by an offshore earthquake. (2) The tsunami propagates and inundates land. (3) Some oil storage tanks move as a result of tsunami inundation flow. (4) Oil is spilled from tsunami-driven tanks at varying locations over time. (5) The spilled oil spreads floating on the tsunami flow. (6) A heat source ignites the floating oil. (7) The fire spreads via the floating oil. Here, we model atmospheric storage tanks with fixed roofs, which store liquids at ambient pressure; other types of storage tanks are not addressed. Therefore, oil spills resulting from liquid sloshing caused by long-period ground motion are neglected. Seismic damage to oil storage tanks and resulting oil spills are not considered because tanks are typically designed to be protected from strong ground motion; however, few measures are implemented to prevent tanks from moving under tsunami inundation. Because oil fires typically emit much radiative energy in all directions, strong radiative heating can extend to distant locations if structures do not block the thermal radiation.

The proposed methodology, therefore, adopts the radiative heat flux as a quantitative measure of the fire hazard. The radiative heat flux changes over time. Therefore, its maximum value in a predefined simulation period is used to quantify the fire hazard. To investigate the probability distribution of this quantity, the proposed methodology considers the following factors as uncertain inputs: (1) the fault slip distribution, (2) the oil filling level of each tank, and (3) the fire starting time and position.

Conversely, earthquake and fire occurrences are deterministically treated by specifying the earthquake magnitude and number of ignition incidents. While the earthquake magnitude and occurrence probability are typically evaluated from historical records and geological and geographical data, the fire occurrence uncertainty is problematic. Similarly to the earthquake occurrence probability, the probability of ignition might also be able to be modeled using data for past tsunami fire

events. While inundated electrical equipment or metals are inferred as possible ignition sources from past tsunami fire events [21,69], hazardous materials as possible ignited fuel are constantly moving and spreading due to the tsunami. With such a complicated ignition mechanism, the ignition modeling may not be straightforward, and in fact, no ignition models are currently available. Because fire hazard assessments vary greatly depending on how the ignition probability is given, it needs to be handled carefully. Therefore, this study assumed that a fire is certain to occur without modeling the ignition probability in order to conservatively assess the fire hazard. Specifically, the proposed methodology assumes that a fire starts at a single location (i.e., the number of ignition incidents is one) and that the time and location of the ignition incident is uncertain.

The fault slip distribution, consisting of an earthquake source model representing the fault rupture characteristics, is an important factor governing tsunami generation and is required to evaluate the water surface elevation resulting from sea bottom deformation, which is used as an initial condition in simulating tsunami propagation and inundation. Therefore, its uncertainty can significantly affect tsunami flow variability. The constantly changing oil filling level of each tank governs the tank movement and oil spills resulting from tsunamis. It determines the total weight of a tank and the static friction between the bottom plate and foundation. These quantities are used as tank movement thresholds for tsunami wave forces acting on a tank. For tanks expected to move, all of the initially stored oil is assumed to eventually spill. Therefore, the oil filling level uncertainty can significantly affect the variability of the spilled oil amount. The fire starting time and position govern the fire spread behavior of the floating oil on the tsunami flow. This information is used as a set of initial conditions when simulating the tsunami-driven oil fire spread. Generally unpredictable, the fire starting time and position need to be treated as uncertain factors.

The probabilistic definition of the fire hazard is represented as the probability that the maximum radiative heat flux q at a specific site resulting from fires exceeds a threshold q_{cr} given that an earthquake with a moment magnitude m occurs and a number of ignition incidents n_F occur (here, n_F is set to one); this is the conditional site-specific exceedance probability of the maximum radiative heat flux resulting from fires. This probability needs to be numerically evaluated via Monte Carlo simulations. Each combination of the above three factors is called a fire scenario, and the probability is computed via numerical simulations for numerous statistically sampled fire scenarios. The probability, or fire hazard equation, can be written as

$$p(q \geq q_{cr}|m, n_F) = \sum_{i=1}^{n_S} [w_i \times I(q_i \geq q_{cr}|m, n_F)], \tag{1}$$

where n_S is the number of fire scenarios, $I(\cdot)$ is an indicator function that takes a value of 1 when the maximum radiative heat flux for the i-th fire scenario q_i is greater than or equal to q_{cr} and takes a value of 0 otherwise, and w_i is the weight coefficient assigned to each fire scenario, where

$$\sum_{i=1}^{n_S} w_i = 1. \tag{2}$$

The threshold value needs to be objectively specified to indicate the potential consequences of strong radiative heating. Here, two values are adopted: 10 kW/m^2, approximately corresponding to the minimum external heat flux required to achieve piloted ignition of wood [57,58], and 2 kW/m^2, approximately corresponding to the human tolerance limit for exposure to radiative heat [59]. The former is introduced to assess the possibility of fire damage to structures or secondary fires related to hazardous installations. Although the critical heat flux for ignition varies among combustible materials, the value for wood is adopted here for simplicity. The latter captures the possibility of skin burn injuries to tsunami evacuees on the rooftops of structures.

2.2. Computational framework

Fig. 2 illustrates the computational framework for evaluating the fire hazard equation. This framework is based on Monte Carlo simulations and implements a series of numerical simulations of tsunami propagation and inundation, tsunami-induced tank movement, and tsunami-driven oil fire spread for numerous stochastically generated scenarios. It has the following nine-step procedure.

(1) Numerous synthetic fault slip distributions (hereinafter, source models) are stochastically generated under a given moment magnitude using empirical subduction earthquake scaling relationships [55]. These correlate the moment magnitude to various macro source parameters, including parameters related to the probability distribution of slip values and their spatial heterogeneity, and other typical parameters (e.g., fault length, fault width, mean slip, and maximum slip). The source models are basically heterogeneous slip models based on random fields with variable fault geometries used as inputs when simulating tsunami propagation and inundation.

(2) Tsunami propagation and inundation simulations are performed for the source models to predict horizontal water flow velocity fields paired with water surface elevation distributions as a function of time. These are required to simulate tsunami-induced tank movement and tsunami-driven oil fire spread. The tsunami simulations calculate initial water surface elevations caused by sea bottom deformation from the source models and numerically solve the horizontal two-dimensional nonlinear long-wave equations. The set of predictions obtained for each source model is called the tsunami sample.

(3) Simulated tsunamis for use in subsequent simulations are selected from the tsunami sample to reduce the time and effort required throughout the assessments. The selection is based on the maximum water surface elevation at a given nearshore location predicted for a given source model (hereinafter, the tsunami height). First, an empirical cumulative distribution function (CDF), describing the percentile rank, is plotted for the tsunami height. Then, several percentile ranks, for which corresponding tsunami heights are linked to source models and other predictions, are specified at equal intervals to select simulated tsunamis with equal weights. These carefully selected simulated tsunamis are representative of the entire population.

(4) Numerous oil filling level patterns for each tank are stochastically generated as inputs for simulating tsunami-induced tank movement. The oil filling levels are treated as independent random variables that are uniformly distributed between the minimum and maximum operative filling levels of the tanks. This treatment reflects the uncertainty in the actual filling level, which may have seasonal and/or spatial correlations. Each generated pattern is called an oil filling pattern.

(5) Tsunami-induced tank movement simulations are performed for combinations of the selected simulated tsunamis and generated oil filling patterns. The simulations predict the presence/absence of movement for each tank using a simplified physics-based model that mathematically formulates the occurrence conditions for floating and sliding, the expected behaviors of tanks subjected to tsunami inundation flow. The locations of tanks predicted to move are predicted as a function of time by approximating the tank behavior as the translational motion of the center of gravity in a horizontal two-dimensional coordinate system. The predicted time-varying tank locations, which represent oil spilling positions, are used as inputs when simulating the tsunami-driven oil fire spread. This step is equivalent to generating numerous oil spill patterns. All the oil initially stored in these tanks is assumed to eventually spill.

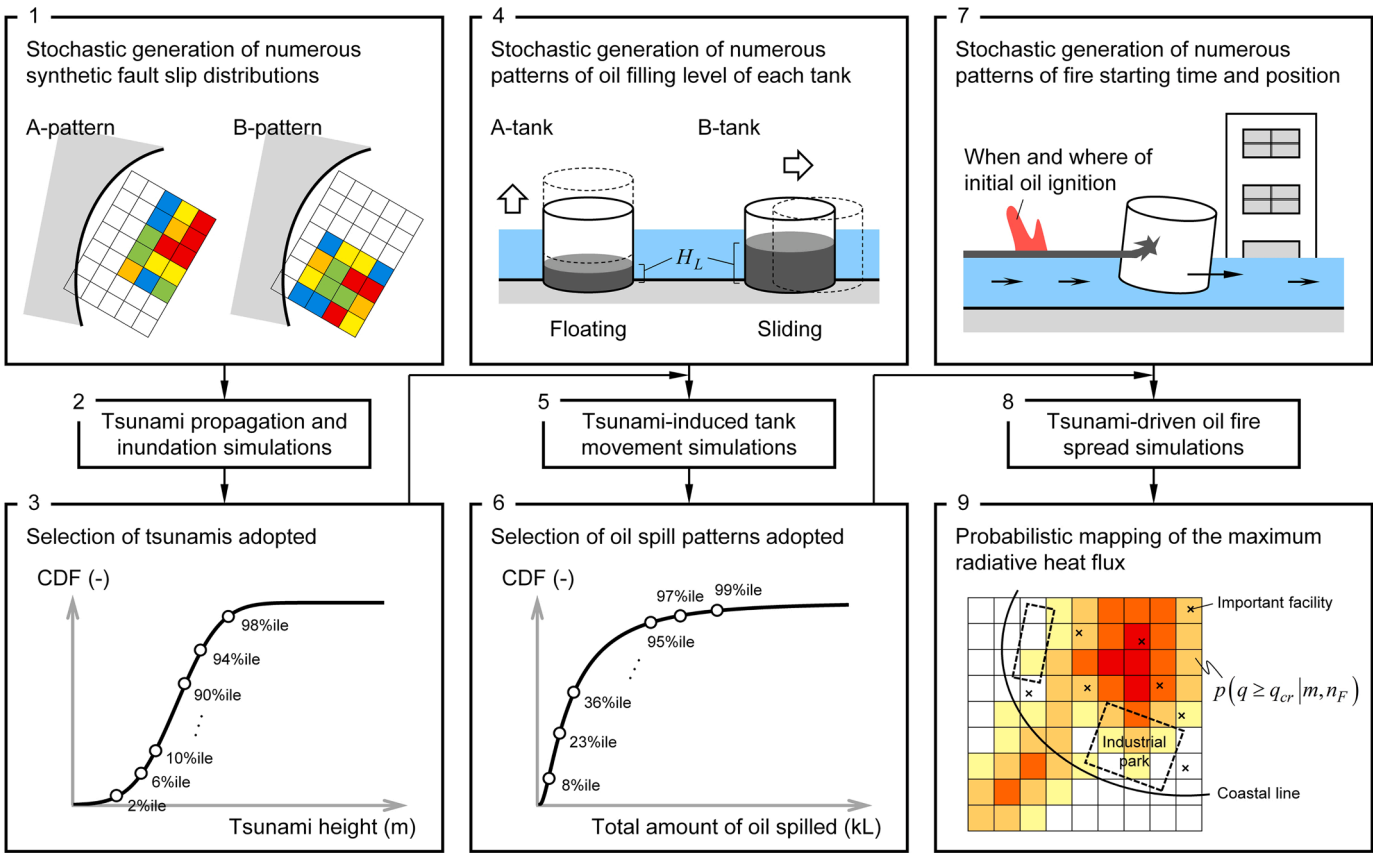

Figure 2. Computational framework for evaluating tsunami-triggered oil spill fire hazards considering associated uncertainties.

(6) Oil spill patterns considered in subsequent simulations are selected from those generated in Step 5 to reduce the time and effort required throughout the assessments. The selection is based on the total amount of oil spilled (i.e., the total amount of oil initially stored in the tanks predicted to move). First, an empirical CDF is plotted for the total amount of oil spilled. Then, several percentile ranks are specified to select oil spill patterns linked to simulated tsunamis. The percentile ranks are specified at shorter intervals in the region with a smaller function gradient and are specified at longer intervals in the region with a larger gradient. Therefore, different interval weight coefficients are assigned to the selected oil spill patterns. These oil spill patterns are representative of the entire population.

(7) Numerous fire starting time and position patterns are stochastically generated to use as inputs when simulating tsunami-driven oil fire spread. First, the fire starting time is randomly determined in a given period. Then, the fire starting position is determined by randomly selecting an initial burning oil particle from the oil particles with ignitable thicknesses at the fire starting time. Each generated pattern is called an oil ignition pattern.

(8) Tsunami-driven oil fire spread simulations are performed for combinations of the selected oil spill patterns and generated oil ignition patterns. The simulations are based on a horizontal two-dimensional Lagrangian model that traces the behavior of individual floating oil particles, including their burning behavior, to describe the overall fire behavior as an assemblage of burning oil particles [14]. The model mathematically formulates the motion of oil particles floating on water during tsunamis and the burning behavior of oil particles, including fire spread between oil particles. The simulations predict the heat release rate of individual oil particles resulting from combustion and their locations as a function of time. The radiative heat flux can then be computed at a given location as a function of time by approximating the flame radiation as isotropic radiation from a point source, enabling an evaluation of the fire hazard equation.

(9) The spatial distribution of the site-specific exceedance probability of the maximum radiative heat flux is visualized as a probabilistic fire hazard map. This mapping is useful for understanding the frequency and locations of exposure to strong radiative heating that can lead to the ignition of combustible materials or skin burns of evacuees on tsunami vertical evacuation structures.

More details concerning the implemented models are given in Section 2.3; however, the framework illustrated in Fig. 2 is flexible and the implemented models can be replaced or improved as appropriate.

2.3. Implemented models

2.3.1. Tsunami source

The tsunami source models are generated using a random phase source modeling approach [e.g., 50–54] based on subduction zone earthquake scaling relationships [55]. Subduction zones are located at interfaces between oceanic and continental plates (Fig. 3). When the leading edge of the overriding plate breaks free and springs seaward, an earthquake occurs along the subduction zone and raises the sea floor and water above it, resulting in a tsunami. The random phase source modeling approach can consider the spatial uncertainty of subduction earthquake ruptures; that is, it considers uncertainty in both the location and geometry of the fault plane and the slip distribution over the fault plane. The scaling relationships represent statistical properties of key source parameters related to the geometry and slip distribution derived from inverted finite-fault rupture models for past subduction earthquakes included in the SRCMOD database [60]. The source parameters include the fault length L, fault width W, mean slip D_a, maximum slip

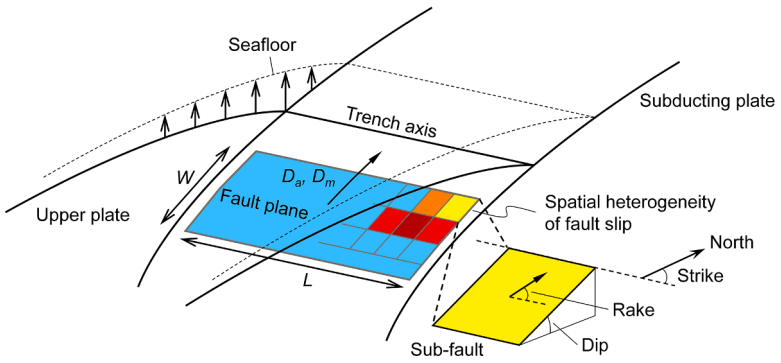

Figure 3. Schematic of a tsunami source model for a megathrust earthquake along a subduction zone.

D_m, Box-Cox parameter λ, correlation length along strike direction A_z, correlation length along dip direction A_x, and Hurst number H. With the strike and dip, the fault length and width determine the fault plane geometry. The source model expresses heterogeneity by dividing the entire fault plane into a finite number of sub-faults and assigning different slip values to each sub-fault. The mean slip, maximum slip, and Box-Cox parameter characterize the statistical properties of the slip values. The correlation lengths and Hurst numbers are used to model the spatial characteristics of the slip distribution. Most source parameters are modeled as a function of the moment magnitude; however, the Box-Cox parameter and Hurst number are modeled as random variables following specific probability distributions independent of the moment magnitude [55]. Additional details can be found in the literature [e.g., 53].

2.3.2. Tsunami propagation and inundation

Tsunami propagation and inundation are numerically simulated using JAGURS [81] that solves the nonlinear shallow water equations using a leap-frog staggered-grid finite difference scheme. This study adopted a non-dispersive model in Cartesian coordinates. The governing equations of motion in two-dimensional space and continuity equation are

$$\frac{\partial M}{\partial t}+\frac{\partial}{\partial x}\left(\frac{M^2}{D}\right)+\frac{\partial}{\partial y}\left(\frac{MN}{D}\right)=-gD\frac{\partial \eta}{\partial x}-\frac{gn^2}{D^{7/3}}M\sqrt{M^2+N^2}, \tag{3}$$

$$\frac{\partial N}{\partial t}+\frac{\partial}{\partial x}\left(\frac{MN}{D}\right)+\frac{\partial}{\partial y}\left(\frac{N^2}{D}\right)=-gD\frac{\partial \eta}{\partial y}-\frac{gn^2}{D^{7/3}}N\sqrt{M^2+N^2}, \tag{4}$$

$$\frac{\partial \eta}{\partial t}+\frac{\partial M}{\partial x}+\frac{\partial N}{\partial y}=0, \tag{5}$$

where η is the water level, M and N are the water fluxes in the x- and y-directions, respectively, g is the gravitational acceleration, D is the total depth, n is the Manning coefficient, and t is time. The initial water surface elevation is evaluated from the tsunami source model using the formulae of Okada [61] and Tanioka and Satake [62]. Nested grid systems are implemented to model the tsunami waves in the deep ocean, over the continental shelf, near shore, and on land. The ocean bottom and land roughness are given by the Manning coefficient. The coefficient on land is based on land use.

2.3.3. Oil filling level of storage tanks

The storage tank oil filling level changes constantly. Survey data for oil storage tanks damaged by the tsunami following the 2011 Tohoku earthquake [63] show that the ratio of the quantity of oil stored at the time of the earthquake to the tank capacity ranged from 0% to 100% without being concentrated in specific regions. Because little information is available concerning the actual filling level variation, the oil filling level for each tank H_L is modeled as an independent random variable that is uniformly distributed between certain bounds, similarly to conventional equipment fragility assessments [e.g., 29,39]. The minimum and maximum operative filling levels are adopted as the lower and upper bounds, respectively.

The oil storage tanks are modeled as simple cylindrical tanks with fixed roofs. If D_T is the tank diameter and $H_{L,\min}$ and $H_{L,\max}$ are the minimum and maximum operative filling levels, respectively (Fig. 4), the amount of oil stored in each tank at the time of an earthquake V_L is

$$V_L=\frac{\pi D_T^2 H_L}{4}=\frac{\pi D_T^2}{4}\left[H_{L,\min}+\phi\left(H_{L,\max}-H_{L,\min}\right)\right], \tag{6}$$

where ϕ is an uniform random number between 0 and 1.

2.3.4. Tsunami-induced tank movement

The presence or absence of tank movement under tsunami inundation is determined by physically formulating the occurrence conditions of the floating and sliding behaviors of the tanks subjected to tsunami inundation flow. Oil storage tanks are assumed to move when at least one of the two occurrence conditions is met. Similarly to conventional equipment fragility assessments [e.g., 29,39], the occurrence conditions are formulated by approximating the tanks, including liquids, as rigid bodies. The tsunami wave forces acting on the tanks vary with time and are divided into vertical $F_V(t)$ and horizontal $\mathbf{F}_H(t)$ components (Fig. 4). The former is compared with the total tank weight to determine the presence/absence of floating, while the latter is compared with the static friction between the bottom plate and foundation to determine the presence/absence of sliding. Hence, the occurrence conditions are

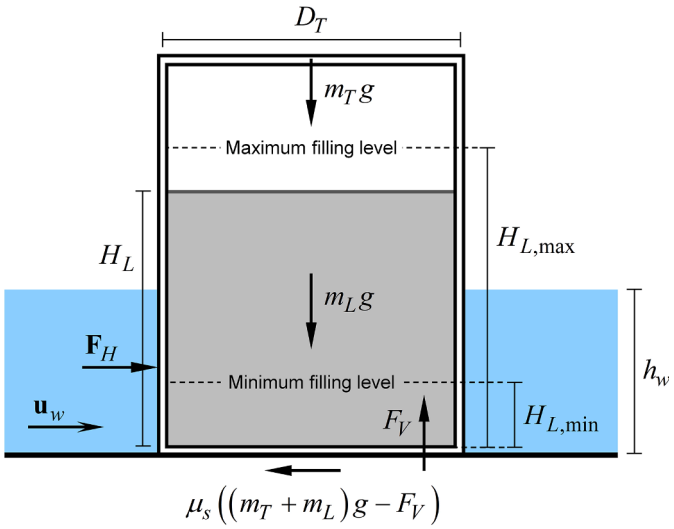

Figure 4. Schematic of a simplified model for oil storage tanks subjected to tsunami inundation flow.

$$\frac{F_V(t)}{(m_T+m_L)g} \geq 1 \tag{7}$$

for floating and

$$\frac{|\mathbf{F}_H(t)|}{\mu_s[(m_T+m_L)g - F_V(t)]} \geq 1 \tag{8}$$

for sliding, where m_T is the tank plate mass, m_L is the oil mass, and μ_s is the coefficient of static friction between the bottom plate and foundation, which is set to 0.5 corresponding to the coefficient for dry stones against soil surfaces [64] and steel materials against concrete surfaces [65].

The tsunami wave forces are determined from the simulated tsunami depth and velocity at a given location. Because the implemented tsunami simulations provide the average cross-sectional flow velocity in the horizontal direction and the water surface elevation, empirical equations are used to compute the tsunami wave forces. According to empirical equation performance investigations via wave basin experiments [40], the measured vertical tsunami wave loads can be roughly predicted using the buoyancy based on the static pressure; the measured horizontal tsunami wave loads can be roughly predicted using the Morison equation even when adopting the horizontal water velocity and water depth measured under the condition without tanks. Accordingly, the tsunami wave forces are computed using the water depth $h_w(t)$ and water flow velocity $\mathbf{u}_w(t)$:

$$F_V(t) = \rho_w g \frac{\pi D_T^2 h_w(t)}{4}, \tag{9}$$

$$\mathbf{F}_H(t) = \frac{1}{2} C_d \rho_w \mathbf{u}_w(t)|\mathbf{u}_w(t)| D_T h_w(t) + C_m \rho_w \frac{\partial \mathbf{u}_w(t)}{\partial t} \frac{\pi D_T^2 h_w(t)}{4}, \tag{10}$$

where ρ_w is the water density, C_d is the drag coefficient, and C_m is the inertia coefficient. The diameter and height of the tanks are neglected in the tsunami simulations, and the water depth and velocity at the points corresponding to the tanks are used. Based on previous investigations [40], values of 1.2 and 2.0 were adopted for C_d and C_m, respectively.

The locations of moving oil storage tanks are predicted as a function of time by numerically solving the equation of motion for each tank. These time-varying locations are required to model oil spills occurring at varying locations over time. Because little information is available concerning oil release behavior from tanks during tsunamis, the modeled oil is released from the tsunami-driven tanks at a constant flow rate and instantaneously floats on the water surface. Similarly to conventional simplified modeling of drifting objects [e.g., 3,66], the tsunami-driven tank motion is approximated as the translational motion of the center of gravity in a horizontal two-dimensional coordinate system. Hence, the equation of motion for each tank is

$$\begin{aligned}(m_T+m_L)\frac{\partial \mathbf{u}_d}{\partial t} &= \frac{1}{2} C_d \rho_w D_T h_d (\mathbf{u}_w - \mathbf{u}_d)|\mathbf{u}_w - \mathbf{u}_d| + \rho_w \frac{\pi D_T^2 h_d}{4} \frac{\partial \mathbf{u}_w}{\partial t} \\ &+ \rho_w (C_m - 1) \frac{\pi D_T^2 h_d}{4} \left(\frac{\partial \mathbf{u}_w}{\partial t} - \frac{\partial \mathbf{u}_d}{\partial t} \right) \\ &- \mu_d \left((m_T+m_L)g - \rho_w g \frac{\pi D_T^2 h_d}{4} \right) \frac{\mathbf{u}_d}{|\mathbf{u}_d|} \qquad (t \geq t_d),\end{aligned} \tag{11}$$

where $\mathbf{u}_d$ is the velocity vector of the tank; h_d is the vertical distance between the tank bottom plate and water surface; μ_d, set to 0.2 [64], is the coefficient of dynamic friction between the tank bottom plate and ground surface; and t_d is the time the tank starts moving. Here, (t) is omitted for variables that are a function of time. The first, second, third, and fourth terms on the right-hand side represent the drag, force resulting from the water flow pressure gradient, effect of added mass, and dynamic friction against the ground surface, respectively. However, Eq. (11) is not applied when the water depth at the predicted location at the next time step is smaller than the vertical distance between the tank bottom plate and water surface at the present time step. In that case, tanks are assumed to stop moving and their velocities are treated as zero.

The draft h_d is

$$h_d = \min\left(\frac{(m_T+m_L)g}{\rho_w g \frac{\pi D_T^2}{4}}, h_w \right). \tag{12}$$

If s is the volume flow rate of oil spilling from a tank, which is assumed to be constant, the oil mass contained in a tank at a given time m_L is

$$m_L = \rho_L[V_L - s(t - t_d)] \qquad (t \geq t_d), \tag{13}$$

where ρ_L is the oil density. The time variation of m_L is reflected in the tank motion via Eqs. (11) and (12). Here, $s = 0.2\ \mathrm{m}^3/\mathrm{s}$, matching the value adopted in a previous numerical investigation of the tsunami fire in Kesennuma Bay following the 2011 Tohoku earthquake [14].

The time-varying position vector of a given tank $\mathbf{X}_d$ is predicted using a formula [66] that represents the displacement of a drifting object as the sum of a displacement determined by the equilibrium of forces and an uncertain displacement resulting from water turbulence, which is modeled as a random walk with turbulent diffusion coefficients:

$$\mathbf{X}_d = \mathbf{X}_d^I + \int_{t_d}^{t} \mathbf{u}_d dt + \sum_{k=n_d}^{n} \sqrt{24\boldsymbol{\kappa}\Delta t}\left(\boldsymbol{\xi}_k - \frac{1}{2}\right) \qquad (t \geq t_d), \tag{14}$$

where $\mathbf{X}_d^I$ is the initial position vector, $\boldsymbol{\kappa}$ is a matrix in which the diagonal elements are turbulent diffusion coefficients while the other elements are zero, n is the present time step, n_d is the time step corresponding to t_d, Δt is the time increment, and $\boldsymbol{\xi}_k$ is a vector of uniform random numbers between 0 and 1. The values of the turbulent diffusion coefficients are calculated based on the results of hydraulic experiments [67].

2.3.5. Fire starting time and position

Fires typically result from contact between flammable/combustible materials and ignition sources. Ignition sources can be categorized into random (e.g., hot surfaces, flames, and sparks) and intentional ignition sources [68]. Various ignition sources are expected during tsunami-related oil spill accidents in and near industrial zones. Heat release in a chemical reaction between metal and seawater is suspected of having caused the ignition of floating oil during the tsunami following the 1964 Niigata earthquake [69]. Meanwhile, burning floating debris is suspected of having caused the ignition of floating oil in Kesennuma Bay during the tsunami following the 2011 Tohoku earthquake [15]. The former ignition incident occurred approximately 5 h after the tsunami arrived [69], while the latter occurred approximately 2 h after the tsunami arrived [15]. Accidental ignition is typically caused by a random ignition source; therefore, when and where ignition occurs is generally unpredictable. Here, the fire starting time is first randomly determined in a given period. Then, the fire starting position is determined by randomly selecting an initial burning oil particle from the oil particles with ignitable thicknesses at the fire starting time.

2.3.6. Tsunami-driven oil fire spread

Tsunami-driven oil fire spread is numerically simulated using a particle-based computational model [14]. The model approximates tsunami-driven oil as an assemblage of floating disc-shaped oil particles with variable thickness and radius and mathematically formulates the motion and burning behavior of individual oil particles to simulate the overall fire behavior (Fig. 5). Key assumptions are the following. (1) Oil and water are clearly separated, and chemical and biological state changes (e.g., dissolution and emulsification) are neglected. (2) Although spilled oil consists of different petroleum products, the

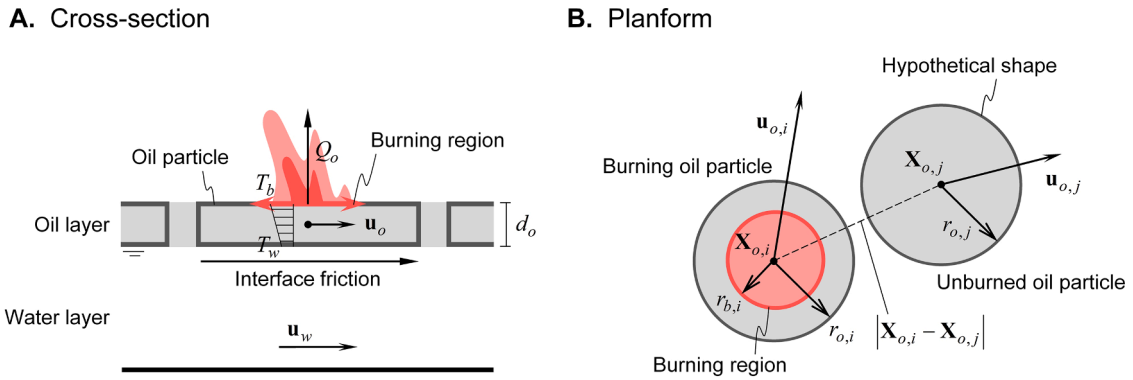

Figure 5. Schematic of a Lagrangian model for tsunami-driven oil fire spread [14].

properties of the spilled oil particles are represented by the petroleum product spilled in the largest volume. Accordingly, the oil particle properties are homogeneous. (3) Oil particles follow the translational motion of the center of gravity in the horizontal direction resulting from the combined effect of the interface friction between oil and water, water turbulence, and spreading resulting from gravity and viscous forces. (4) The burning region of each oil particle expands concentrically on the surface from its center at a rate depending on its thickness. (5) Fires spread from burning oil particles to unburned oil particles when burning regions contact the edges of unburned oil particles. (6) Fires are self-extinguished when the thickness of burning oil particles becomes smaller than 1 mm. Tsunami-driven oil particle locations are predicted as a function of time in a horizontal two-dimensional coordinate system. Simultaneously, the burning area and the heat release rate resulting from combustion are predicted as a function of time for each oil particle, as is fire spread between oil particles.

The time-varying locations of tsunami-driven oil particles are predicted similarly to the tank movement modeling described in Section 2.3.4. The position vector of a given oil particle $\mathbf{X}_o$ is

$$\mathbf{X}_o = \mathbf{X}_o^I + \int_{t_s}^{t} \mathbf{u}_o dt + \Delta\mathbf{X}_w + \Delta\mathbf{X}_s \qquad (t \geq t_s), \tag{15}$$

$$\Delta\mathbf{X}_w = \sum_{k=n_s}^{n} \sqrt{24\kappa\Delta t}\left(\boldsymbol{\xi}_k - \frac{1}{2}\right), \tag{16}$$

$$\Delta\mathbf{X}_s = C_p(t-t_s)^{1/4}\sqrt{\Delta t}\begin{bmatrix}\cos(2\pi\zeta_1)\\ \sin(2\pi\zeta_2)\end{bmatrix}, \tag{17}$$

where $\mathbf{X}_o^I$ is the initial position vector, $\Delta\mathbf{X}_w$ is the stochastic displacement representing the effect of water turbulence, $\Delta\mathbf{X}_s$ is the stochastic displacement representing the oil spreading effect caused by gravity and viscous forces, $\mathbf{u}_o$ is the oil particle velocity vector determined by the force equilibrium, t_s is the time to spill for an oil particle, n_s is the time step corresponding to t_s, C_p is the spreading coefficient, and ζ_1 and ζ_2 are uniform random numbers between 0 and 1. Eq. (17) is taken from Ref. [70], where C_p was found to be 0.115 in hydraulic experiments.

Assuming that the oil–water interface friction is proportional to the square of the relative oil–water velocity, the equation of motion for each oil particle is

$$m_o\frac{\partial\mathbf{u}_o}{\partial t} = C_f\rho_o A_o(\mathbf{u}_w - \mathbf{u}_o)|\mathbf{u}_w - \mathbf{u}_o|, \tag{18}$$

where m_o is the oil particle mass, ρ_o is the oil particle density, A_o is the oil particle contact area with water, and C_f is the interface friction coefficient. Because m_o is represented as $\rho_o A_o d_o$ using the oil particle thickness d_o, the time derivative of the oil particle velocity is inversely proportional to the oil particle thickness. Based on hydraulic experiments, C_f is set to 0.006 [71].

The oil particle thickness varies depending on the ambient particle number density. Here, the volume-weighted number of oil particles per unit area is evaluated for each square grid cell. This grid-cell-based number density $\overline{d_{cell}}$ is adopted as the oil particle thickness d_o:

$$d_o \equiv \overline{d_{cell}}, \quad \overline{d_{cell}} = \frac{\sum \delta_{cell} V_o}{b^2}, \tag{19}$$

where V_o is the oil particle volume, b is the cell width, and δ_{cell} is a dummy variable that takes a value of 1 when a given oil particle exists in the cell and takes a value of 0 otherwise.

The oil particle radius r_o is determined by the oil particle volume and thickness:

$$r_o = \sqrt{\frac{A_o}{\pi}} = \sqrt{\frac{V_o/d_o}{\pi}}. \tag{20}$$

Let r_b be the radius of the burning region of a given oil particle. The time derivative of r_b (i.e., the flame spread rate) is modeled as a function of the oil particle thickness based on the results of fire experiments that investigated the flame spread rate over oil floating on static water for kerosene and crude oil [17–19]:

$$\frac{\partial r_b}{\partial t} = \begin{cases} 1.2d_o + 0.0016 & (0.001 \leq d_o < 0.007) \\ 0.01 & (0.007 \leq d_o) \end{cases}. \tag{21}$$

Eq. (21) represents an experimental tendency: the flame spread rate is approximately constant when floating oil is thick but becomes smaller when floating oil is thinner because the convective flow mechanism of floating oil changes. It is unclear whether this equation is applicable to different types of oil; however, except for gasoline and similar oils, its application is not thought to cause significant problems because the flame spread rate is much lower than the travel velocity of oil transported by tsunamis.

The heat release rate of a given oil particle Q_o is

$$Q_o = \Delta H_o \dot{m}_b(\pi r_b^2), \tag{22}$$

where $\dot{m}_b$ is the mass loss rate per unit area of a given oil particle and ΔH_o is the heat of combustion. Here, $\dot{m}_b$ is computed by adding the heat loss to water to the results of pool fire experiments without a water layer:

$$\dot{m}_b = \dot{m}_{b,pool} - \frac{1}{L_v}\left\{\frac{k_o(T_b - T_w)}{d_o}\right\}, \tag{23}$$

where $\dot{m}_{b,pool}$ is the mass loss rate per unit area derived from pool fire experiments without a water layer, T_b is the boiling point of oil, T_w is the water temperature, k_o is the effective heat transfer coefficient, and L_v is the heat of vaporization. The effective heat transfer coefficient k_o is

$$k_o = \left(\frac{\dot{m}_{b,pool}L_v}{T_b - T_w}\right)d_{\min}, \tag{24}$$

because it is assumed that $\dot{m}_b$ becomes zero when the oil particle thickness decreases to the minimum ignitable thickness $d_{\min}$.

The volume loss rate resulting from the combustion of a given oil particle is

$$\frac{\partial V_o}{\partial t} = -\left(\frac{Q_o}{\Delta H_o \rho_o}\right). \tag{25}$$

If i and j indicate burning and unburned oil particles, respectively, the occurrence condition of fire spread between oil particles is

$$\left|\mathbf{X}_{o,i} - \mathbf{X}_{o,j}\right| \le r_{b,i} + r_{o,j} \quad \text{and} \quad d_{o,j} \ge 0.001\,, \tag{26}$$

where the positional relationship between two circles is considered.

2.3.7. Thermal radiation from flames

The radiative heat flux at a given location resulting from fires is evaluated using a point heat source modeling approach similarly to Ref. [72]. The model approximates a flame formed above a burning region as a point heat source that radiates uniformly in all directions (Fig. 6). This simplified model is widely used in fire safety engineering [73]. The point heat source model is within 5% of the correct radiative heat flux when the distance from the source is over 2.5 times larger than the diameter of the fire [74].

Assume that flames are formed individually above each burning oil particle. Consider a given heat receiving surface with a unit area. Because the radiative energy released from a flame is typically given by multiplying the heat release rate by the radiative fraction χ_R, the total radiative heat flux incident to the receiving surface from all flames above burning oil particles q is

$$q = \sum_k \frac{\chi_R Q_{o,k}}{4\pi s_k^2} \cos\theta_k, \tag{27}$$

where k indicates a burning oil particle, s_k is the distance from the point source to the receiving surface, and θ_k is the angle of incidence. Here, χ_R is set to 0.3 because data from large pool fire experiments show that the radiative fraction averagely increases with the decreasing diameter of the pool fire but is up to approximately 30% [73].

Because information concerning the potential horizontal extent of strong radiative heating is sufficient to make risk management decisions, the horizontal distance is substituted into s_k neglecting the vertical distance, that is, the point source height above the burning surface and the receiving surface height are not modeled. Additionally, θ_k is assumed to be zero for all point sources, that is, the inclination of the receiving surface is not explicitly specified, because it is impossible to uniquely determine the inclination of the receiving surface in advance such that the total incident heat flux becomes the largest for point sources with time-varying locations. These assumptions overestimate the fire hazard; however, this conservative estimation is preferred from a risk management perspective. Similarly, the radiation blocking effect of structures is neglected. Note that the radiative heat flux predicted using Eq. (27) varies with time because the locations and heat release rates of burning oil particles change over time; however, its maximum value in a predefined simulation period for a given scenario is used as the value of q_i when evaluating the fire hazard equation.

3. Numerical setup

The PTFHA is illustrated via a realistic case study of possible offshore megathrust earthquakes in the Nankai Trough subduction zone off the coast of Japan. Earthquakes with magnitudes of 7.9–8.6 have occurred in various regions along this subduction zone at intervals of approximately 100–200 years since at least 1400 years ago. Therefore, there is a high probability that an earthquake with a similar magnitude will occur somewhere along this subduction zone at some point in the near future [75]. Because improving preparedness against imminent earthquakes is a serious priority of national and local governments in Japan, deterministic tsunami hazard and consequence assessments have been conducted under the assumption of a subduction zone earthquake with Mw 9.1, a worst-case magnitude [76]. These governmental assessments do not cover fire analyses and provide no information on how frequently predicted results could occur. The case study here also assumes the occurrence of Mw 9.1 earthquakes but incorporates fire analyses and associated uncertainties to better understand possible tsunami-related Natech events.

We synthesized 300 fault slip distributions for Mw 9.1 earthquakes along the Nankai Trough subduction zone using the scaling relationships [55]. The subduction zone geometry was modeled using data from the Central Disaster Management Council of the Japanese Government [76]. Fig. 7 shows examples of synthesized fault slip distributions demonstrating that random phase modeling successfully generates various heterogeneous slip models with different fault geometries. Because the magnitude is extremely large, the synthesized slip models have extensive fault planes and cover most of the subduction zone. Some slip models have clusters of large slip regions on the eastern or western sides of the fault planes, while others have large slip regions scattered over the fault planes or forming a belt-like distribution along the trench axis ranging from the eastern to western sides; however, the large slip regions are primarily concentrated in shallow and/or slightly deep locations. Differences in the fault slip distribution can produce tsunami flows with various characteristics.

The Port of Osaka, Japan, is approximately 200 km from the Nankai Trough and includes a petrochemical industrial park made up of 14 companies storing or handling large amounts of oil or high-pressure gas spanning an area of 3.5 km^2 (Fig. 8). The total amount of oil stored or handled is approximately 274,000 kL [77]. Residential and commercial areas of Osaka, the second largest city in Japan, are located in the

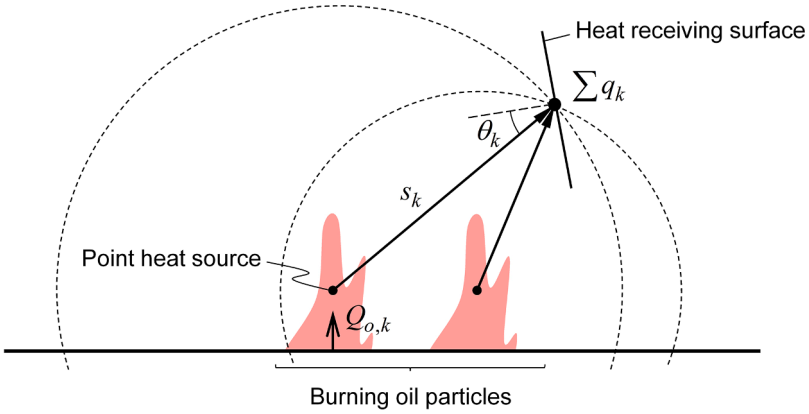

Figure 6. Schematic of a point source model for radiation heat transfer from flames.

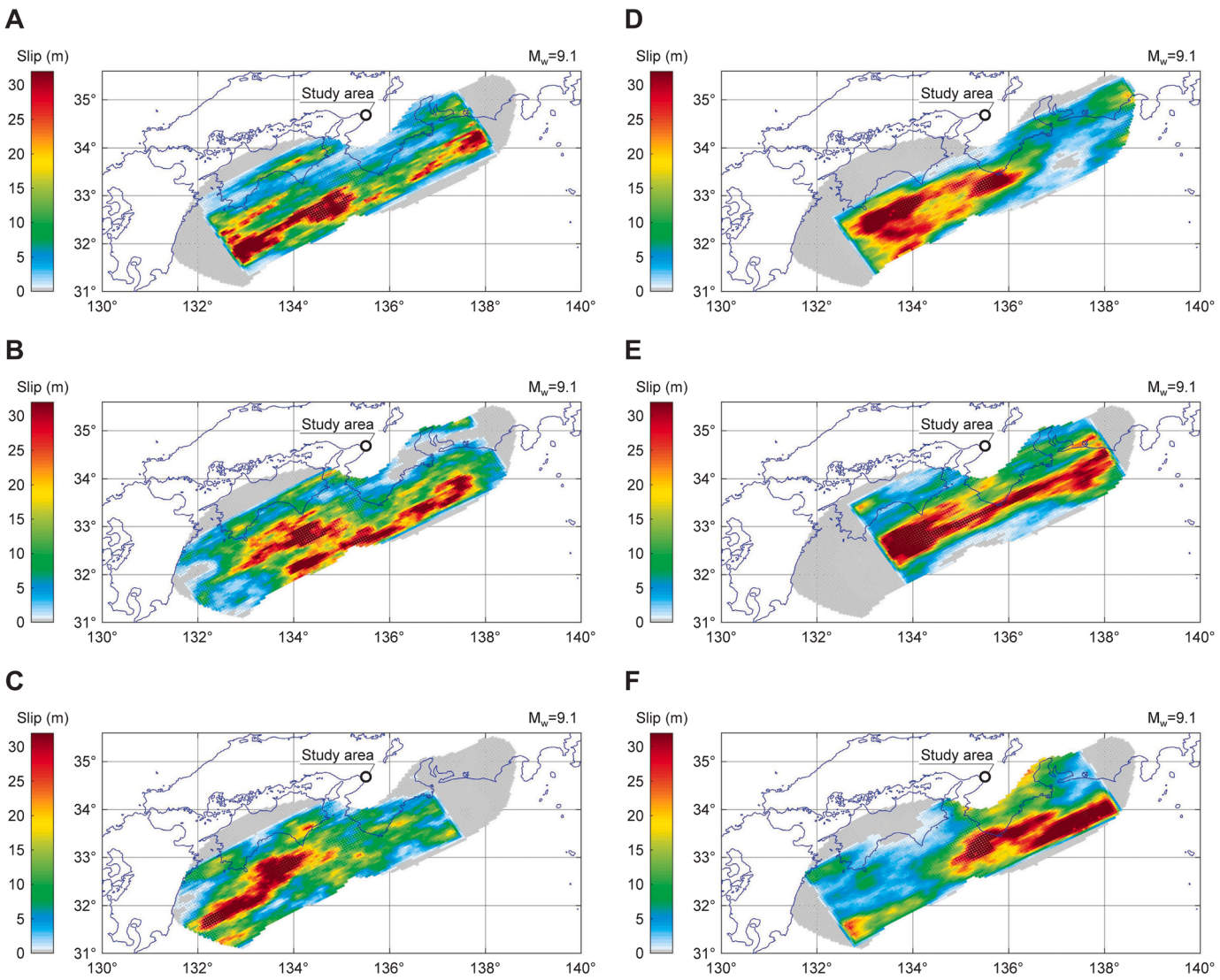

Figure 7. Examples of synthesized fault slip distributions for Mw 9.1 earthquakes in the Nankai Trough subduction zone.

vicinity of the industrial park. A number of designated buildings for vertical evacuation are available to elevate evacuees above the level of tsunami inundation. These are reinforced concrete or steel reinforced concrete buildings constructed after 1982 with three or more stories.

Detailed information concerning individual oil storage tanks in the industrial park are based on a questionnaire survey mailed to the 14 companies on November 1, 2021. Respondents were individuals in charge of handling or safety inspection or knowledgeable of management conditions. The questionnaires gathered data concerning each oil storage tank, including the location, weight, diameter, type and name of petroleum product stored, legal storage capacity (excluding unavailable and contingency spaces), and self-imposed maximum and minimum operative filling levels. The type and name of the petroleum product stored were used to determine its density. When this information was unreported, a density of 820 kg/m^3 was adopted as a representative value. When the operative filling levels were unreported, filling levels corresponding to the legal storage capacity and the floor level were adopted as the maximum and minimum, respectively. The response rate was approximately 57%, with eight completed questionnaires collected before December 3, 2021. For the remaining companies, tank locations and diameters were determined by scanning aerial photographs provided by the Geospatial Information Authority of Japan. The tank heights were determined based on a 2-m-resolution digital surface model produced by an aerial light detection and ranging company, and the weights were estimated assuming the tank plate thickness and material density. The legal storage capacity was estimated based on Japanese hazardous material regulations. For other items, assumed values were adopted.

A total of 231 oil storage tanks are considered in the case study, slightly larger than the official count (213) as of March 2022 [77]. Although the case study is not based on exact data, it does represent the actual situation; therefore, the case study results are sufficient to support decision-making in Natech risk management. The oil storage tanks in this industrial park are all atmospheric storage tanks with fixed roofs, with 52% being small-scale tanks with a legal storage capacity less than 500 kL.

Tsunami propagation and inundation simulations were performed for the 300 synthesized fault slip models. A simulation period of 10 h from the time of the earthquake was adopted with a time increment of 0.1 s. Five nested domains, with grid sizes of 810, 270, 90, 30, and 10 m were adopted to the computational domains from fault to land. Bathymetry and topography were modeled using data from the Central Disaster Management Council of the Japanese Government [76]. The mean sea level of Tokyo Bay was used as the reference level to treat the bathymetric depths and topographic elevations in an integrated manner. Tidal changes were neglected because the date and time of earthquake

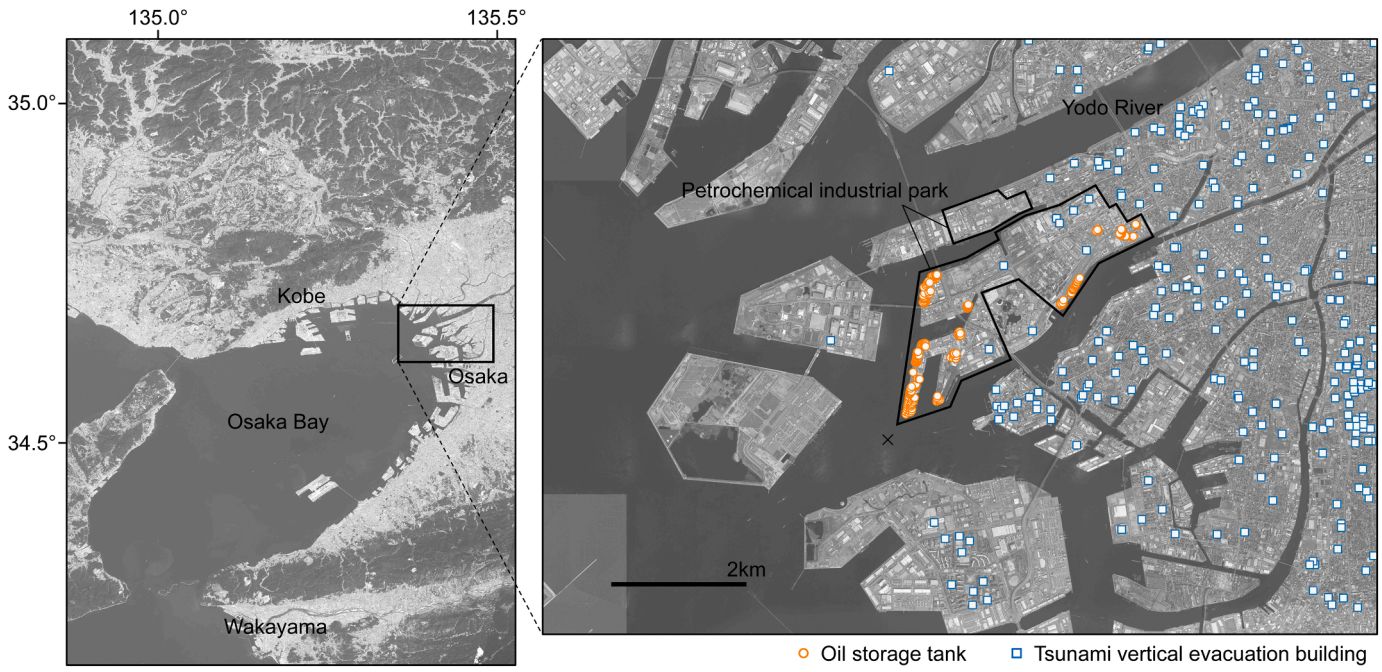

Figure 8. Overview of the Port of Osaka, Japan (data overlaid on the aerial photograph provided by the Geospatial Information Authority of Japan).

occurrence are unknown. The bottom friction at the sea floor was evaluated using the Manning formula and its roughness coefficient. The resistance of land structures was evaluated using the Manning formula, and the roughness coefficient was selected according to the land use type. Coastal floodgates were assumed to be completely closed before the tsunami waves arrived because there is expected to be approximately 2 h warning. Conversely, the effect of seawalls was neglected to avoid underestimating tsunami inundation flow because seawalls may be destroyed by seismic ground motion before tsunami waves hit. The empirical CDF for the tsunami height (simulated at the location marked with a cross in Fig. 8) is shown in Fig. 9. The simulated tsunami heights range from approximately 0.52 m to 2.75 m above the mean sea level; the expected value is approximately 1.75 m. This indicates that, even if an extremely large earthquake occurs in the subduction zone, tsunami waves will hardly run up on land in some cases while they will cause extensive flooding in others. This is apparent in the inundation maps for typical percentile-ranked simulated tsunamis (Fig. 10). For subsequent simulations, 25 simulated tsunamis were selected corresponding to percentile ranks from 2% to 98% at 4% intervals.

We generated 1000 oil filling patterns for use in the tsunami-induced tank movement simulations, with the oil filling level randomly determined between the minimum and maximum operative filling levels for each tank. Tsunami-induced tank movement simulations were performed for combinations of the 25 simulated tsunamis and the 1000 oil filling patterns. Then, 26 combinations were selected for subsequent simulations based on the empirical CDF for the total amount of oil spilled. The selected combinations correspond to typical percentile ranks (specifically, 8%, 23%, 36%, 45%, 51%, 57%, 61%, 63%, 65%, 67%, 69%, 71%, 73%, 75%, 77%, 79%, 81%, 83%, 85%, 87%, 89%, 91%, 93%, 95%, 97%, and 99%) and have different weight coefficients corresponding to the intervals. The simulation period was 10 h, starting at the earthquake occurrence. The time increment was 0.6 s. Tsunami predictions for every minute were used as inputs and were linearly interpolated when simulating tsunami-induced tank movement to reduce the effort required to transfer the tsunami simulation data. Simulated waveforms with a time increment of 1 s were only applied when predicting which oil storage tanks started moving.

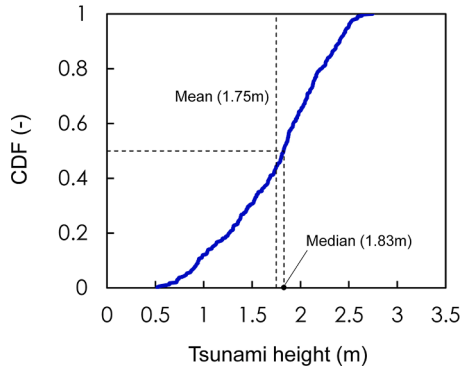

Figure 9. Empirical cumulative distribution function (CDF) for the tsunami height in the 300 tsunami simulations for Mw 9.1 earthquakes in the Nankai Trough subduction zone.

We considered 40 fire starting time and position patterns for each oil spill pattern; therefore, a total of 1040 tsunami-driven oil fire spread simulations were performed. The fire starting time was randomly determined between 150 min and 240 min after the earthquake because (1) tsunami simulations indicate that tsunami waves arrive at the study area approximately 120 min after an earthquake regardless of fault slip model and (2) preliminary analyses indicate that fires hardly spread after 300 min because, even in the largest oil spill case, the oil thickness becomes very thin with increasing spreading area. To reduce the computational time, the simulation period of the tsunami-driven oil fire spread was set to 6 h following the time of the earthquake. The time increment was 0.6 s. Tsunami predictions for every minute were also used as inputs and were linearly interpolated as in the tsunami-induced tank movement simulations. The oil particle properties were represented by those of diesel oil, with a density, boiling point, heat of vaporization, and heat of combustion of 820 kg/m^3, 603 K, 250 kJ/kg, and 42000 kJ/kg, respectively. The mass loss rate per unit area under conditions without heat loss to water was set to 0.045 kg/s/m^2 based on pool fire experiments [78]. The initial oil particle volume was uniformly set to 0.06 m^3.

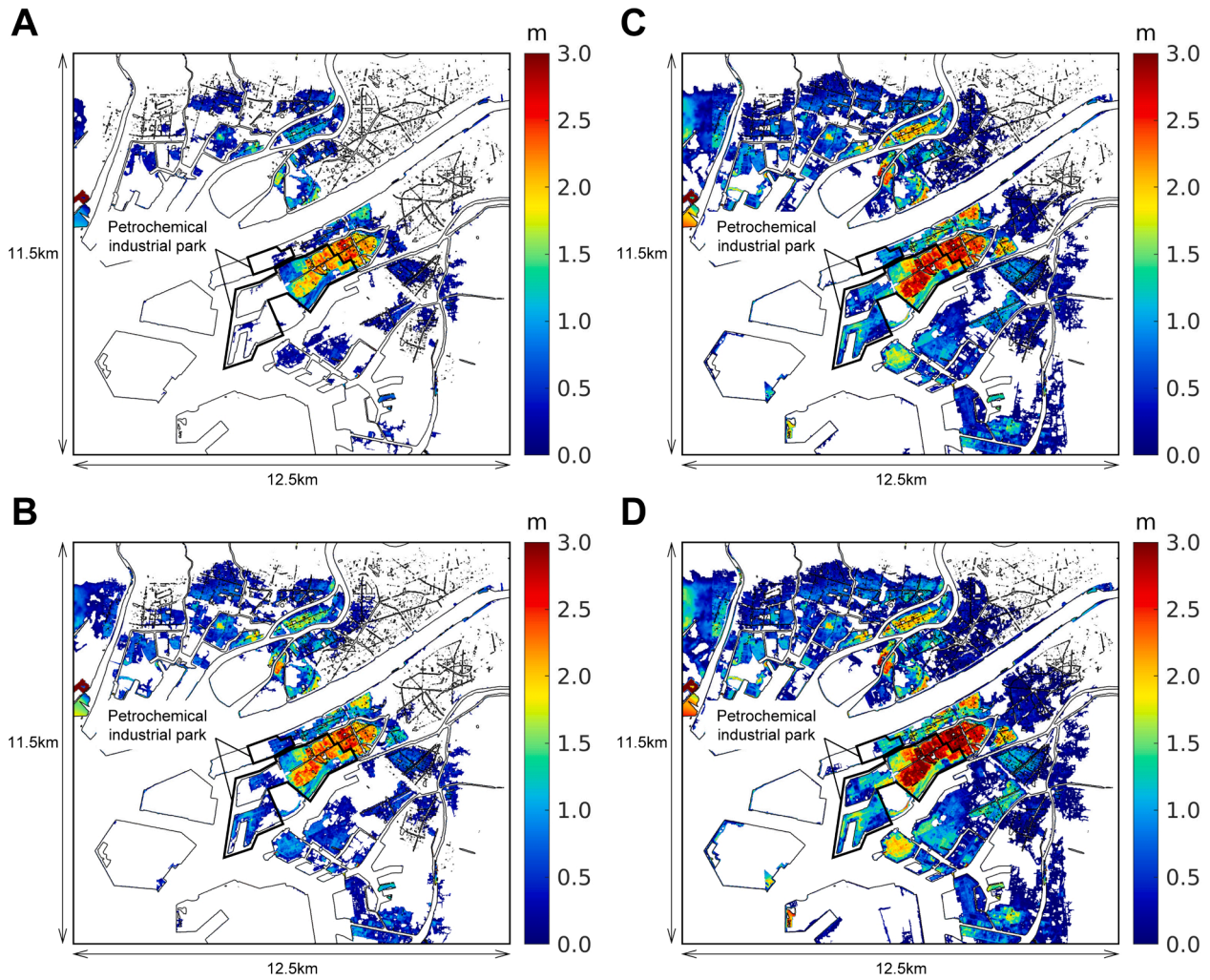

Figure 10. Inundation depth distributions for (A) 14, (B) 50, (C) 86, and (D) 98 percentile-ranked simulated tsunamis.

4. Results and discussion

4.1. Examples of simulated tsunami-driven oil fire spreading

First, several examples of simulated tsunami-driven oil fire spreading are shown to demonstrate the time sequence of tsunami arrival, inundation, oil storage tank movement, oil spreading, and fire spreading. Fig. 11 shows examples where a total of 2044 kL of oil was spilled, corresponding to the 99 percentile of the 25,000 oil spill patterns. The simulated tsunami in the examples had a height of 2.46 m above the mean sea level at the nearshore location, corresponding to the 94 percentile of the 300 simulated tsunamis.

The simulated tsunami arrived approximately 120 min after the earthquake and inundated the industrial park and surrounding area (Fig. 11). Ultimately, 223 of 231 oil storage tanks were inundated and 30 started moving. Some oil storage tanks drifted in the ocean to the west, while others drifted in the inundation area on land to the east. Because oil was spilled continuously while the tanks drifted, oil spreading areas formed in both the ocean and the inundation area on land in the vicinity of the tsunami-driven tanks. Because the tsunami flow field changed over time, the tsunami carried the floating oil particles in various directions and expanded the oil spreading areas with time. The fire initiated with oil particles floating in the bay around 162 min after the earthquake and then spread consecutively to surrounding oil particles. The burning area reached its peak around 183 min after the earthquake; subsequently, the fire decayed gradually because the oil thickness thinned with increasing oil spreading area over time. The peak burning area, approximately 2.9 ha, was much smaller than the inundation area. The complex tsunami flow field significantly contributed to the fire development; that is, the tsunami transported and diffused burning oil particles and the fire moved constantly while changing its burning area. This qualitative behavior is consistent with that of the tsunami fire in Kesennuma Bay following the 2011 Tohoku earthquake [14]. Although the fire started in the bay in these examples, there were also cases where the fire started in the inundation area on land.

4.2. Variability of the total amount of oil spilled

Fig. 12 shows the relationship between the predicted number of oil storage tanks flooded or moved and the 25 selected tsunami scenarios. The number of flooded oil storage tanks is uniquely determined for each tsunami scenario, while the number of moved oil storage tanks varies because 1000 oil filling patterns were considered for each tsunami scenario. As expected, the number of flooded oil storage tanks increases nearly monotonically with increasing tsunami height, ranging from 68 to 223 (from approximately 29% to 97% of the total). The number of moved oil storage tanks varies similarly; that is, the expected value increases nearly monotonically from 3.0 to 34.6 (from approximately 1% to 15% of the total) with increasing tsunami height, with the difference between the maximum and minimum values reaching 31.

Fig. 13 shows the empirical CDF for the total amount of oil spilled for the 25,000 tsunami-induced tank movement simulations. There is

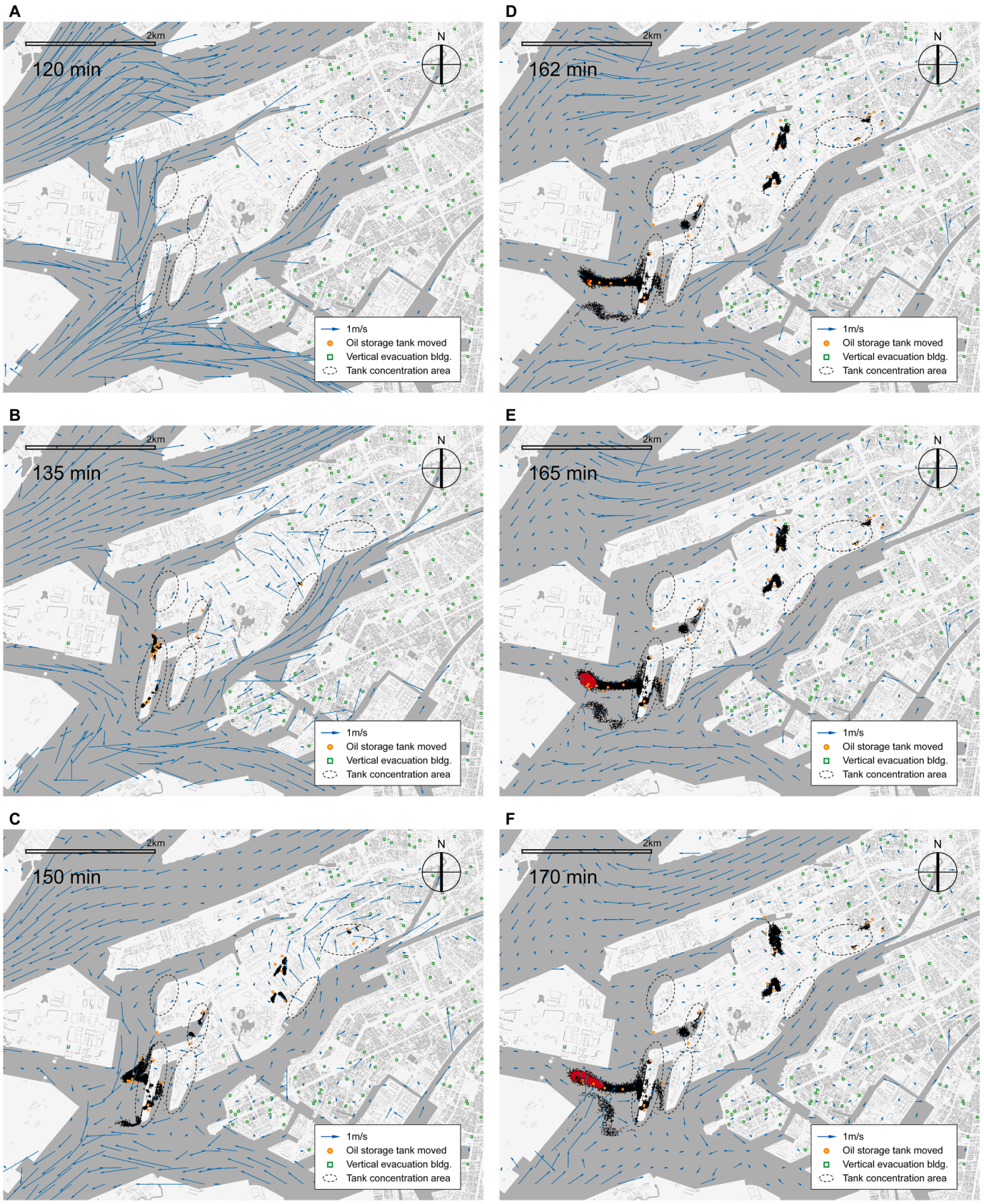

Figure 11. Examples of simulated tsunami-driven oil fire spreading (blue arrows represent tsunami flow velocity vectors; black and red particles represent unburned and burning oil particles, respectively).

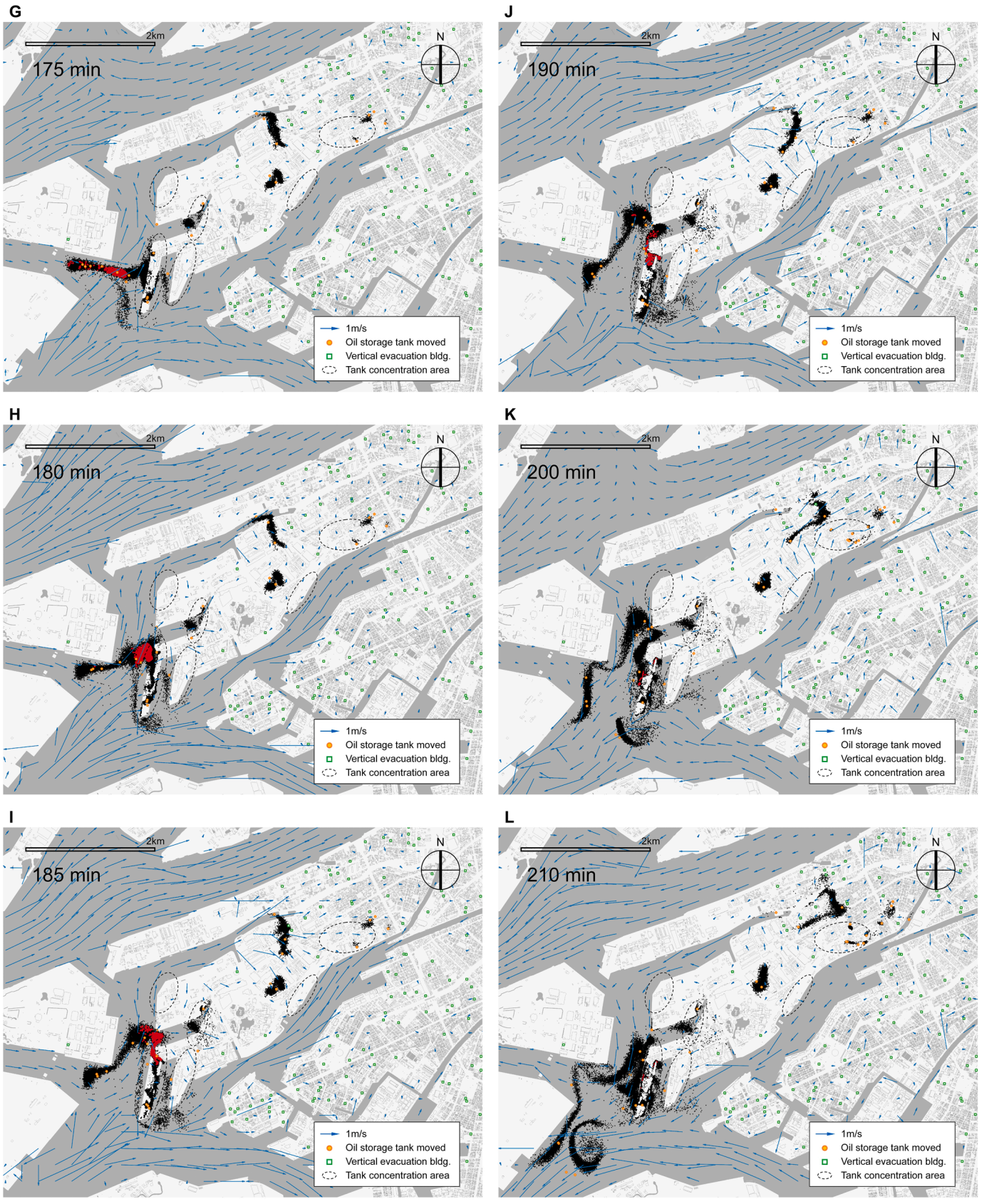

Figure 11. (*continued*).

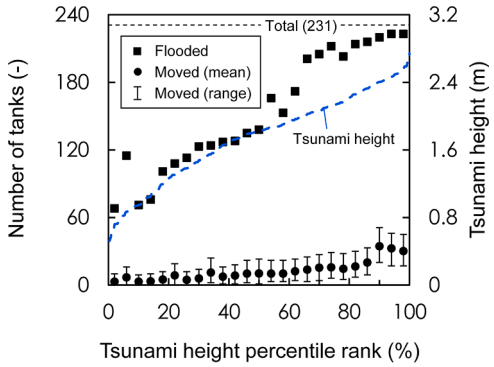

Figure 12. Relationship between the predicted number of oil storage tanks flooded or moved and the 25 selected tsunami scenarios.

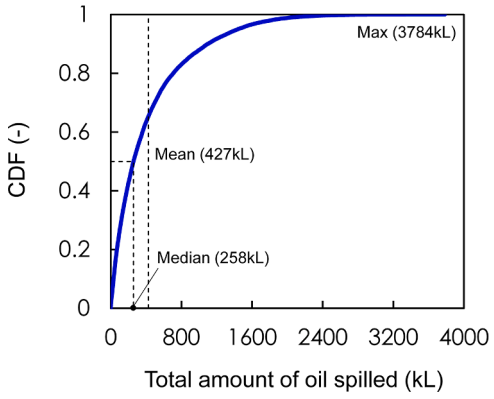

Figure 13. Empirical cumulative distribution function (CDF) for the total amount of oil spilled in the 25,000 tsunami-induced tank movement simulations.

significant variation in the total amount of oil spilled, ranging from 0 to approximately 3784 kL, with an expected value of approximately 472 kL. The CDF has a large gradient when the total amount of oil spilled is small and a small gradient when the total amount of oil spilled is large. This indicates that small oil spills will occur in most cases even if an extremely large earthquake occurs, but large oil spills are possible, though less frequent. The local government deterministically estimated a total spilled oil amount of 4452 kL [77]. However, such a large oil spill is highly unlikely according to our results. Therefore, the proposed methodology could deepen stakeholders' understanding of possible tsunami-related Natech events. The conservative governmental estimate was based on a single specific tsunami scenario and assumed that each oil storage tank was filled to a level at which the spill amount was maximized.

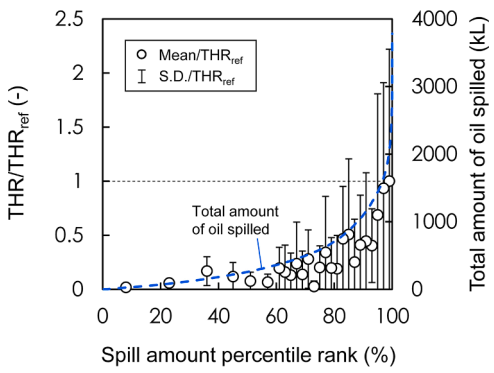

Figure 14. Relationship between the total heat release (THR) of simulated fires and the total amount of oil spilled.

4.3. Variability of the fire scale

Fig. 14 shows the relationship between the total heat release (THR) of simulated fires and the total amount of oil spilled. The THR represents the amount of heat energy released from a fire during its burning time (the integrated heat release rate over time) and can measure the scale of simulated fires with different starting times and development. The THR values are plotted for 1040 tsunami-driven oil fire spread simulations. Because the THR values (up to 10^7 MJ) are so large, values relative to the mean THR for the 99 percentile-ranked oil spill pattern are plotted instead. As expected, THR is roughly correlated with the total amount of oil spilled, with the fire scale becoming larger with increasing amounts of oil spilled. In addition, the dispersion relative to the mean, resulting from fire starting time and position uncertainties, generally becomes larger with increasing amounts of oil spilled.

4.4. Probabilistic fire hazard maps

Fig. 15 shows the probabilistic fire hazard maps obtained via 1040 tsunami-driven oil fire spread simulations. The maps display the spatial distributions of the conditional exceedance probability of the maximum radiative heat flux with two threshold values of 10 kW/m^2 and 2 kW/m^2.

The potential extent of strong radiative heating is concentrated in the industrial park and its vicinity, including the bay and the land, and forms two clusters on the western and eastern sides. The cluster on the western side is centered on areas where oil storage tanks are concentrated, while that on the eastern side is located away from the tank concentration areas and extends to residential areas outside the industrial park. However, the potential extent of strong radiative heating is limited compared with the potential tsunami inundation areas shown in Fig. 10. This result (i.e., the concentrated fire impact) suggests clear characteristics for areas where oil is liable to be transported by tsunamis. A pathline analysis, which allows a transient flow to be followed in a Lagrangian manner and traces massless particles to record the fluid evolution with time, supports this finding. Fig. 16 shows the spatial distribution of the time-averaged number of tracer particles obtained from the analysis with the mean value for the 25 selected tsunami scenarios plotted. The procedure was as follows. (1) Tracer particles were released from the initial oil storage tank locations. (2) The number of tracer particles per minute was counted using a 200-m grid. (3) The average number of particles for each grid during the period from 150 min to 360 min after the earthquake was calculated. (4) The mean value was calculated by performing steps (1)–(3) for all 25 tsunami scenarios. This analysis roughly estimates spatial differences in the degree of how long and how much oil exists in a region of interest. The obtained distribution highlights areas where oil is liable to be transported by tsunamis. This distribution approximately corresponds to the fire hazard map with a threshold value of 10 kW/m^2 but differs slightly from the map with a threshold value of 2 kW/m^2. This difference is due to the effect of the thermal radiation from fires. Because the radiative heat flux decreases with increasing distance from a fire source, fire hazard maps with smaller threshold values extend to larger areas than the possible burning areas. Therefore, the fire hazard map with a threshold value of 2 kW/m^2 is more extensive than areas where the time-averaged number of tracer particles is large.

The fire hazard maps suggest the following potential consequences including frequency information. (1) In high fire hazard areas, where the probability of exceeding 10 kW/m^2 is 5%–20%, tsunami fires might ignite flammable/combustible materials and cause secondary fires to structures that remain after tsunami waves hit, such as buildings, plants, and hazardous installations. Fire spread to hazardous installations could result in catastrophic damage to the industrial park and surrounding area. (2) Ten tsunami vertical evacuation buildings are included within

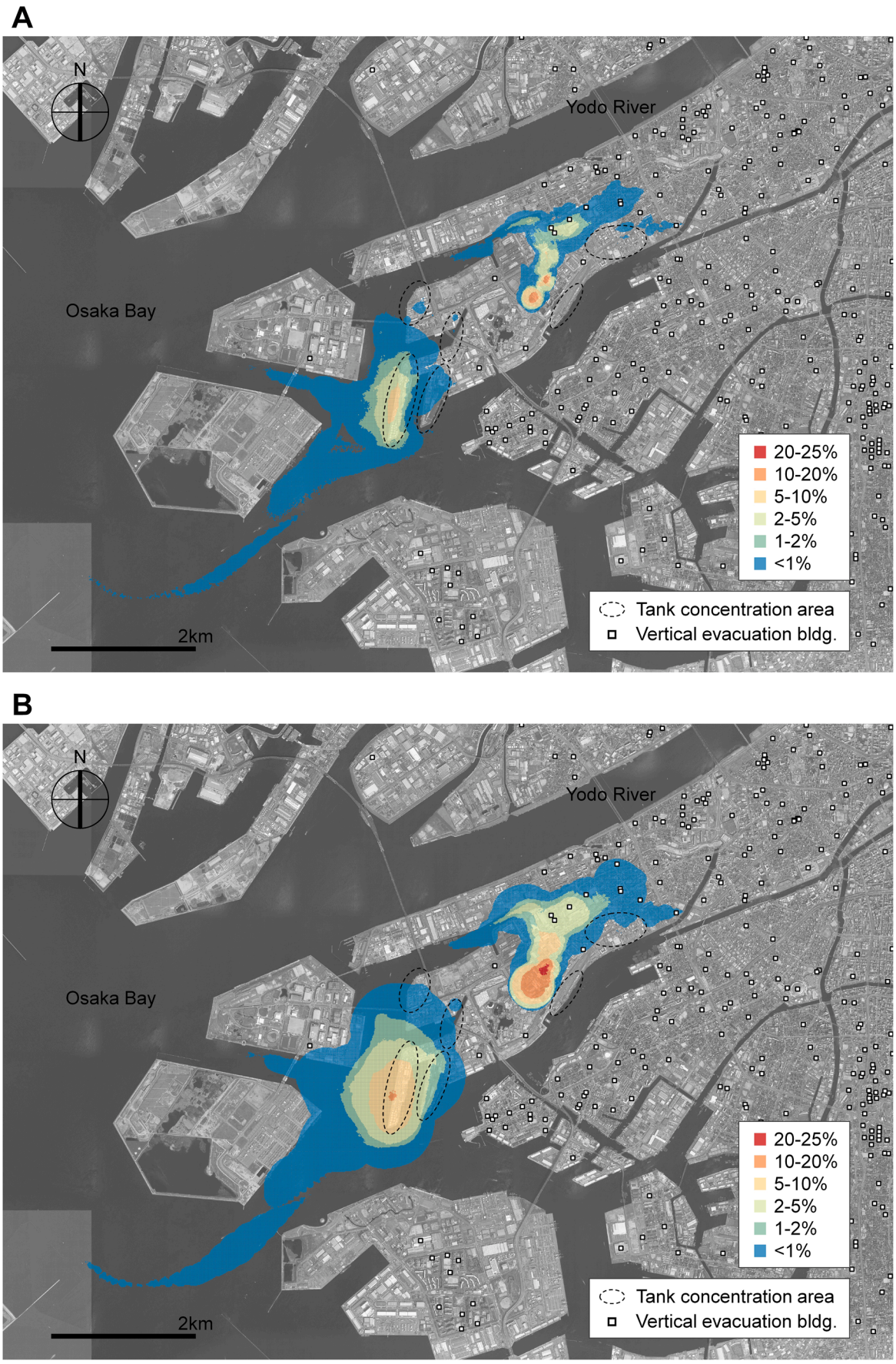

Figure 15. Probabilistic fire hazard maps obtained via 1040 tsunami-driven oil fire spread simulations: spatial distributions of the conditional exceedance probability of the maximum radiative heat flux with threshold values of (A) 10 kW/m^2 and (B) 2 kW/m^2.

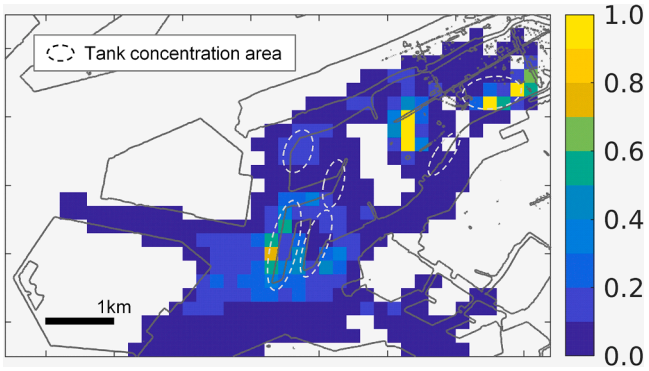

Figure 16. Spatial distribution of the time-averaged number of tracer particles obtained from a pathline analysis (mean value for the 25 selected tsunami scenarios).

the potential extent of strong radiative heating. However, the probability of exceeding 10 kW/m^2 or 2 kW/m^2 is less than 5%. Therefore, tsunami fires are not likely to cause the ignition of tsunami vertical evacuation buildings or skin burns to evacuees on their rooftops if typical building fire protection measures are implemented and sufficient refuge spaces are available indoors.

These useful suggestions demonstrate that the proposed methodology can serve as a tool for understanding potential tsunami fire risks and promoting stakeholder decision-making concerning possible fire risk reduction measures, which is not possible with typical tsunami risk management. Recall that the case study neglected the effect of seawalls on tsunamis; therefore, the evaluated fire hazards are likely overestimated. This is conservative from a risk management perspective. If seawalls work well, the corresponding fire hazards will decrease significantly.

4.5. Fire risk reduction measures

The case study results indicate the possibility of devastating consequences of tsunami-triggered oil spill fires. Such consequences will not occur frequently in this study area even if an extremely large subduction zone earthquake occurs. However, the possibility is not negligible and the numerical results show a probabilistic but coherent fire hazard configuration. Therefore, measures to reduce potential fire risks need to be implemented. Possible fire risk reduction measures include tsunami barriers, flood gate operation, management of hazardous materials, and fire protection of tsunami vertical evacuation buildings.

As for tsunami barriers, seawalls and flood gates existing in the study area can effectively reduce the tsunami impact on oil storage tanks. They can also reduce the amount of oil spilled and the resulting fire impact. As for the management of hazardous materials, spill prevention measures for hazardous materials are effective. While tanks are typically designed to be protected from strong ground motion, few measures are implemented to prevent oil storage tanks from moving under tsunami inundation. Therefore, it is important to individually determine the minimum operative filling level for each oil storage tank considering possible tsunami wave forces; that is, it is important to ensure the minimum weight required to keep a tank from moving under possible tsunami wave forces by controlling the filling level. It is also important to install emergency shutoff valves and develop a system to ensure their closure. This increases the reliability of preventing oil spills. For tsunami vertical evacuation buildings, it is important to ensure that the structural components, exterior walls, and openings of these buildings are fire-resistant and that these buildings have fire compartments to contain any indoor fires within a limited area.

5. Conclusions

A comprehensive PTFHA methodology was developed in the context of Natech risk reduction. The methodology is based on integrated modeling of tsunami propagation and inundation, tsunami-induced movement of oil storage tanks and resulting oil spills, tsunami-driven oil fire spread, and thermal radiation from fires. It incorporates uncertainties in the fault slip distribution, oil filling level of storage tanks, and fire starting time and position into a probabilistic mapping of the maximum radiative heat flux as a quantitative measure of the fire hazard. Its application was illustrated through a realistic case study focusing on possible offshore Mw 9.1 earthquakes. In contrast to typical tsunami direct impact assessments, the results highlight the cascading effects of tsunamis, particularly the large variability in key output variables concerning oil spills and fires, and demonstrate the usefulness of probabilistic fire hazard maps to better understand potential consequences of fires. This methodology can promote reasonable stakeholder decision-making for Natech risk reduction. The case study results include some limitations; therefore, there is room for improvement. The effect of seawalls was neglected because seawalls might be destroyed by seismic ground motion before tsunami waves hit. However, if seawalls remain standing and work well, the total amount of oil spilled and fire hazards will decrease relative to the study results. The case study also assumed that a Mw 9.1 earthquake occurs in the Nankai Trough subduction zone. However, an earthquake with a different magnitude may occur instead. This needs to be investigated in future work by incorporating uncertainty in the earthquake occurrence. Additionally, the probability of ignition was not modeled, and a fire was assumed to be certain to occur in order to conservatively assess the fire hazard. Ignition probability models need to be developed in future work to complete the PTFHA. Furthermore, explosions and other types of fires related to hazardous materials, such as tank fires and ship fires, were not considered. Further improvements to the proposed methodology are essential for appropriate tsunami-triggered cascading disaster assessments and risk reduction.

Funding

This work was partially supported by the Center Research (2022A-01) funded by the Disaster Prevention Research Institute, Kyoto University, and by the Core-to-Core Collaborative Research Program (2023-K-1-2-8) of the Earthquake Research Institute at The University of Tokyo, and the Disaster Prevention Research Institute at Kyoto University, funded by the Ministry of Education, Culture, Sports, Science, and Technology (MEXT) of Japan.

CRediT authorship contribution statement

Tomoaki Nishino: Conceptualization, Methodology, Software, Formal analysis, Writing – original draft, Writing – review & editing, Visualization, Project administration. **Takuya Miyashita:** Conceptualization, Methodology, Software, Formal analysis, Writing – review & editing, Visualization. **Nobuhito Mori:** Conceptualization, Methodology, Writing – review & editing, Project administration.

Declaration of Competing Interest

The authors declare that they have no known competing financial interests or personal relationships that could have appeared to influence the work reported in this paper.

Data availability

The data that has been used is confidential.

Acknowledgments

This work was partially supported by the Center Research (2022A-01) funded by the Disaster Prevention Research Institute, Kyoto University, and by the Core-to-Core Collaborative Research Program (2023-K-1-2-8) of the Earthquake Research Institute at The University of Tokyo, and the Disaster Prevention Research Institute at Kyoto University, funded by the Ministry of Education, Culture, Sports, Science, and Technology (MEXT) of Japan. The authors are grateful to the eight companies that completed the oil storage tank questionnaire. The authors also thank Mizuki Nakano for assistance with the data preparation and Edanz for editing a draft of this manuscript.

Supplementary materials

Supplementary material associated with this article can be found, in the online version, at doi:10.1016/j.ress.2023.109789.

References

[1] Hokugo A, Nishino T, Inada T. Tsunami fires after the Great East Japan earthquake. J Disaster Res 2013;8(4):584–93. https://doi.org/10.20965/jdr.2013.p0584.
[2] Mori N, Takahashi T, Yasuda T, Yanagisawa H. Survey of 2011 Tohoku earthquake tsunami inundation. Geophys Res Lett 2011;38:L00G14. https://doi.org/10.1029/2011GL049210.
[3] Nishino T, Imazu Y. Modeling of the drift and accumulation of tsunami-driven combustible objects: towards tsunami-induced fire spread simulation. Fire Technol 2016;52:1159–78. https://doi.org/10.1007/s10694-015-0519-5.
[4] Lee S, Davidson R, Ohnishi N, Scawthorn C. Fire following earthquake—reviewing the state-of-the-art of modeling. Earthq Spectra 2008;24:933–67. https://doi.org/10.1193/1.2977493.
[5] Tugnoli A, Scarponi GE, Antonioni G, Cozzani V. Quantitative assessment of domino effect and escalation scenarios caused by fragment projection. Reliab Eng Syst Saf 2022;217:108059. https://doi.org/10.1016/j.ress.2021.108059.
[6] Cousins J, Thomas G, Heron D, Smith W. Probabilistic modeling of post-earthquake fire in Wellington, New Zealand. Earthq Spectra 2012;28:553–71. https://doi.org/10.1193/1.4000002.
[7] Lan M, Gardoni P, Qin R, Zhang X, Zhu J, Lo S. Modeling NaTech-related domino effects in process clusters: a network-based approach. Reliab Eng Syst Saf 2022;221:108329. https://doi.org/10.1016/j.ress.2022.108329.
[8] Lan M, Gardoni P, Weng W, Shen K, He Z, Pan R. Modeling the evolution of industrial accidents triggered by natural disasters using dynamic graphs: a case study of typhoon-induced domino accidents in storage tank areas. Reliab Eng Syst Saf 2023;109656. https://doi.org/10.1016/j.ress.2023.109656.
[9] Misuri A, Landucci G, Cozzani V. Assessment of safety barrier performance in the mitigation of domino scenarios caused by Natech events. Reliab Eng Syst Saf 2021;205:107278. https://doi.org/10.1016/j.ress.2020.107278.
[10] Coar M, Sarreshtehdari A, Garlock M, Khorasani NE. Methodology and challenges of fire following earthquake analysis: an urban community study considering water and transportation networks. Nat Hazards 2021;109:1–31. https://doi.org/10.1007/s11069-021-04795-6.
[11] Misuri A, Landucci G, Cozzani V. Assessment of risk modification due to safety barrier performance degradation in Natech events. Reliab Eng Syst Saf 2021;212:107634. https://doi.org/10.1016/j.ress.2021.107634.
[12] Misuri A, Ricci F, Sorichetti R, Cozzani V. The effect of safety barrier degradation on the severity of primary Natech scenarios. Reliab Eng Syst Saf 2023;235:109272. https://doi.org/10.1016/j.ress.2023.109272.
[13] Nishino T. Probabilistic urban cascading multi-hazard risk assessment methodology for ground shaking and post-earthquake fires. Nat Hazards 2023;116:3165–200. https://doi.org/10.1007/s11069-022-05802-0.
[14] Nishino T, Imazu Y. A computational model for large-scale oil spill fires on water in tsunamis: simulation of oil spill fires at Kesennuma Bay in the 2011 Great East Japan earthquake and tsunami. J Loss Prev Process Ind 2018;54:37–48. https://doi.org/10.1016/j.jlp.2018.02.009.
[15] Kesennuma-Motoyosi Fire Department. Record for firefighting activities after the Great East Japan earthquake. 2012. Available at: https://km-fire.jp/wordpress/wp-content/uploads/2020/10/higashikatudou.pdf (accessed 22 July 2022).
[16] Nishino T, Suzuki H, Tsuchihashi T. Basic experiment on the heat release property of a tsunami fire fueled by debris and fuel oil spilled on the sea surface following tsunami. Fire Saf Sci 2014;11:758–68. https://doi.org/10.3801/IAFSS.FSS.11-758.
[17] Arai M, Saito K, Altenkirck RA. Flame propagation over a layer of crude oil floating on water. Int Chem Eng 1993;33:129–35.
[18] Guo J, Lu SX, Zhou JB, Li MH, Wang CJ. Experimental study of flame spread over oil floating on water. Chin Sci Bull 2012;57:1083–7. https://doi.org/10.1007/s11434-011-4959-0.
[19] Kuwana S, Tamizu H, Ito A, Torikai H. Flame spread over liquid fuel on a water layer – basic research on tsunami fire. Open J Saf Sci Technol 2017;7:11–21. https://doi.org/10.4236/ojsst.2017.71002.
[20] Hokugo A, Nishino T, Inada T. Damage and effects caused by tsunami fires: fire spread, fire fighting and evacuation. Fire Sci Technol 2011;30:117–37. https://doi.org/10.3210/fst.30.117.
[21] National Board of Fire Underwriters and Pacific Fire Rating Bureau. The Alaska earthquake, March 27, 1964. San Francisco, Calif.: 1964.
[22] Iwabuchi Y, Koshimura S, Imamura F. Study on oil spread caused by the 1964 Niigata earthquake tsunami. J Disaster Res 2006;1:157–68. https://doi.org/10.20965/jdr.2006.p0157.
[23] Showalter PS, Myers MF. Natural disasters in the United States as release agents of oil, chemicals, or radiological materials between 1980–1989: analysis and recommendations. Risk Anal 1994;14:169–82. https://doi.org/10.1111/j.1539-6924.1994.tb00042.x.
[24] Ricci F, Casson Moreno V, Cozzani V. A comprehensive analysis of the occurrence of NaTech events in the process industry. Process Saf Environ Prot 2021;147:703–13. https://doi.org/10.1016/j.psep.2020.12.031.
[25] Antonioni G, Spadoni G, Cozzani V. A methodology for the quantitative risk assessment of major accidents triggered by seismic events. J Hazard Mater 2007;147:48–59. https://doi.org/10.1016/j.jhazmat.2006.12.043.
[26] Girgin S, Krausmann E. RAPID-N: rapid Natech risk assessment and mapping framework. J Loss Prev Process Ind 2013;26:949–60. https://doi.org/10.1016/j.jlp.2013.10.004.
[27] Alessandri S, Caputo AC, Corritore D, Giannini R, Paolacci F, Phan HN. Probabilistic risk analysis of process plants under seismic loading based on Monte Carlo simulations. J Loss Prev Process Ind 2018;53:136–48. https://doi.org/10.1016/j.jlp.2017.12.013.
[28] Kabir G, Suda H, Cruz AM, Giraldo FM, Tesfamariam S. Earthquake-related Natech risk assessment using a Bayesian belief network model. Struct Infrastruct Eng 2019;15:725–39. https://doi.org/10.1080/15732479.2019.1569070.
[29] Landucci G, Antonioni G, Tugnoli A, Cozzani V. Release of hazardous substances in flood events: damage model for atmospheric storage tanks. Reliab Eng Syst Saf 2012;106:200–16. https://doi.org/10.1016/j.ress.2012.05.010.
[30] Antonioni G, Landucci G, Necci A, Gheorghiu D, Cozzani V. Quantitative assessment of risk due to NaTech scenarios caused by floods. Reliab Eng Syst Saf 2015;142:334–45. https://doi.org/10.1016/j.ress.2015.05.020.
[31] Khakzad N, Gelder PV. Vulnerability of industrial plants to flood-induced Natechs: a Bayesian network approach. Reliab Eng Syst Saf 2018;169:403–11. https://doi.org/10.1016/j.ress.2017.09.016.
[32] Rossi L, Moreno VC, Landucci G. Vulnerability assessment of process pipelines affected by flood events. Reliab Eng Syst Saf 2022;219:108261. https://doi.org/10.1016/j.ress.2021.108261.
[33] Caratozzolo V, Misuri A, Cozzani V. A generalized equipment vulnerability model for the quantitative risk assessment of horizontal vessels involved in Natech scenarios triggered by floods. Reliab Eng Syst Saf 2022;223:108504. https://doi.org/10.1016/j.ress.2022.108504.
[34] Necci A, Antonioni G, Cozzani V, Krausmann E, Borghetti A, Nucci CA. A model for process equipment damage probability assessment due to lightning. Reliab Eng Syst Saf 2013;115:91–9. https://doi.org/10.1016/j.ress.2013.02.018.
[35] Necci A, Antonioni G, Cozzani V, Krausmann E, Borghetti A, Nucci CA. Assessment of lightning impact frequency for process equipment. Reliab Eng Syst Saf 2014;130:95–105. https://doi.org/10.1016/j.ress.2014.05.001.
[36] Necci A, Antonioni G, Bonvicini S, Cozzani V. Quantitative assessment of risk due to major accidents triggered by lightning. Reliab Eng Syst Saf 2016;154:60–72. https://doi.org/10.1016/j.ress.2016.05.009.
[37] Cruz AM, Krausmann E, Franchello G. Analysis of tsunami impact scenarios at an oil refinery. Nat. Hazards 2011;58:141–62. https://doi.org/10.1007/s11069-010-9655-x.
[38] Krausmann E, Cruz AM. Impact of the 11 march 2011, great East Japan earthquake and tsunami on the chemical industry. Nat. Hazards 2013;67:811–28. https://doi.org/10.1007/s11069-013-0607-0.
[39] Basco A, Salzano E. The vulnerability of industrial equipment to tsunami. J Loss Prev Process Ind 2017;50:301–7. https://doi.org/10.1016/j.jlp.2016.11.009.
[40] Araki S, Kunimatsu W, Nishiyama S, Furuse T, Aoki S, Kotake Y. Experimental study on tsunami wave load acting on storage tank in coastal area. J Loss Prev Process Ind 2017;50:347–54. https://doi.org/10.1016/j.jlp.2016.10.004.
[41] Kyaw WP, Sugiyama M, Takagi Y, Suzuki H, Kato N. Numerical analysis of tsunami-triggered oil spill from industrial parks in Osaka Bay. J Loss Prev Process Ind 2017;50:325–36. https://doi.org/10.1016/j.jlp.2017.04.026.
[42] Nishino T, Takagi Y. Numerical analysis of tsunami-triggered oil spill fires from petrochemical industrial complexes in Osaka Bay, Japan, for thermal radiation hazard assessment. Int J Disaster Risk Reduct 2020;42:101352. https://doi.org/10.1016/j.ijdrr.2019.101352.
[43] Mori N, Goda K, Cox D. Recent process in probabilistic tsunami hazard analysis (PTHA) for mega thrust subduction earthquakes. Santiago-Fandino V, Sato S, Maki N, Iuchi K, editors.. The 2011 Japan earthquake and tsunami: reconstruction and restoration. Switzerland: Springer; 2017. p. 469–85. https://doi.org/10.1007/978-3-319-58691-5_27.
[44] Mori N, Satake K, Cox D, Goda K, Catalan PA, Ho TC, Imamura F, Tomiczek T, Lynett P, Miyashita T, Muhari A, Titov V, Wilson R. Giant tsunami monitoring, early warning and hazard assessment. Nat. Rev. Earth Environ. 2022;3:557–72. https://doi.org/10.1038/s43017-022-00327-3.
[45] Geist EL, Parsons T. Probabilistic analysis of tsunami hazards. Nat. Hazards 2006;37:277–314. https://doi.org/10.1007/s11069-005-4646-z.
[46] Annaka T, Satake K, Sakakiyama T, Yanagisawa K, Shuto N. Logic-tree approach for probabilistic tsunami hazard analysis and its applications to the Japanese coasts. Pure Appl Geophys 2007;164:577–92. https://doi.org/10.1007/s00024-006-0174-3.

[47] Horspool N, Pranantyo I, Griffin J, Latief H, Natawidjaja DH, Kongko W, Cipta A, Bustaman B, Anugrah SD, Thio HK. A probabilistic tsunami hazard assessment for Indonesia. Nat Hazards Earth Syst Sci 2014;14:3105–22. https://doi.org/10.5194/nhess-14-3105-2014.
[48] Fukutani Y, Suppasri A, Imamura F. Stochastic analysis and uncertainty assessment of tsunami wave height using a random source parameter model that targets a Tohoku-type earthquake fault. Stoch Environ Res Risk Assess 2015;29:1763–79. https://doi.org/10.1007/s00477-014-0966-4.
[49] Park H, Cox DT. Probabilistic assessment of near-field tsunami hazards: inundation depth, velocity, momentum flux, arrival time, and duration applied to Seaside, Oregon. Coast Eng 2016;117:79–96. https://doi.org/10.1016/j.coastaleng.2016.07.011.
[50] Goda K, Mai PM, Yasuda T, Mori N. Sensitivity of tsunami wave profiles and inundation simulations to earthquake slip and fault geometry for the 2011 Tohoku earthquake. Earth Planets Space 2014;66:105. https://doi.org/10.1186/1880-5981-66-105.
[51] Davies G, Horspool N, Miller V. Tsunami inundation from heterogeneous earthquake slip distributions: evaluation of synthetic source models. J Geophys Res Solid Earth 2015;120:6431–51. https://doi.org/10.1002/2015JB012272.
[52] Mori N, Mai PM, Goda K, Yasuda T. Tsunami inundation variability from stochastic rupture scenarios: application to multiple inversions of the 2011 Tohoku, Japan earthquake. Coast Eng 2017;127:88–105. https://doi.org/10.1016/j.coastaleng.2017.06.013.
[53] Mori N, Muhammad A, Goda K, Yasuda T, Ruiz-Angulo A. Probabilistic tsunami hazard analysis of the Pacific Coast of Mexico: case study based on the 1995 Colima earthquake tsunami. Front Built Environ 2017;3:34. https://doi.org/10.3389/fbuil.2017.00034.
[54] Miyashita T, Mori N, Goda K. Uncertainty of probabilistic tsunami hazard assessment of Zihuatanejo (Mexico) due to the representation of tsunami variability. Coast Eng J 2020;62:413–28. https://doi.org/10.1080/21664250.2020.1780676.
[55] Goda K, Yasuda T, Mori N, Maruyama T. New scaling relationships of earthquake source parameters for stochastic tsunami simulation. Coast Eng J 2016;58:1650010. https://doi.org/10.1142/S0578563416500108.
[56] Gutenberg B, Richter CF. Frequency of earthquakes in California. Bull Seismol Soc Am 1944;34:185–8. https://doi.org/10.1785/BSSA0340040185.
[57] Janssens ML. A thermal model for piloted ignition of wood including variable thermophysical properties. Fire Saf Sci 1991;3:167–76. https://doi.org/10.3801/IAFSS.FSS.3-167.
[58] Tran HC, White RH. Burning rate of solid wood measured in a heat release rate calorimeter. Fire Mater 1992;16:197–206. https://doi.org/10.1002/fam.810160406.
[59] Purser DA, McAllister JL. Assessment of hazards to occupants from smoke, toxic gases, and heat. Hurley MJ, Gottuk D, Hall JR, Harada K, Kuligowski E, Puchovsky M, Torero J, Watts JM, Wieczorek C, editors.. SFPE handbook of fire protection engineering. 5th Edition. New York: Springer; 2016. p. 2378–9.
[60] Mai PM, Thingbaijam KK. SRCMOD: an online database of finite-fault rupture models. Seismol Res Lett 2014;85:1348–57. https://doi.org/10.1785/0220140077.
[61] Okada Y. Surface deformation due to shear and tensile faults in a half-space. Bull Seismol Soc Am 1985;75:1135–54. https://doi.org/10.1785/BSSA0750041135.
[62] Tanioka Y, Satake K. Tsunami generation by horizontal displacement of ocean bottom. Geophys Res Lett 1996;23:861–4. https://doi.org/10.1029/96GL00736.
[63] Hatayama K. Damage to oil storage tanks from the 2011 M_w 9.0 Tohoku-Oki Tsunami. Earthq Spectra 2015;31:1103–24. https://doi.org/10.1193/050713EQS120M.
[64] Fire and Disaster Management Agency. Investigation report on tsunami and inundation measures for hazardous facilities. 2009. Available at: https://www.fdma.go.jp/pressrelease/houdou/items/h21/2105/210526-1houdou/02_stunami_houkokusyo.pdf (accessed 6 October 2022).
[65] Watanabe T, Ozawa J, Oono H, Kitamura T, Tsuruda K. Experimental research into steel material and concrete friction. Tokyu Constr Tech Rep 2007;32:25–8. in Japanese.
[66] Goto T. Numerical analysis of diffusion of timbers by tsunami. In: Proceedings of the 30th Coastal Engineering Symposium; 1983. p. 594–7. in Japanese.
[67] Elder JW. The dispersion of marked fluid in turbulent shear flow. J Fluid Mech 1959;5:544–60. https://doi.org/10.1017/S0022112059000374.
[68] Kljenak I, Bentaib A, Jordan T. Early containment failure. Nuclear Safety in Light Water Reactors. Elsevier; 2012. https://doi.org/10.1016/B978-0-12-388446-6.00003-4.
[69] Zama S. Earthquake and oil storage tank (part 2): damage of hazardous materials facilities and seismic ground motions in the 1964 Niigata earthquake. Saf Tomorrow 2017;174:38–45. in Japanese.
[70] Matsuzaki Y, Fujita I. Experimental study on mechanical spreading of oil on the water surface and application of numerical simulation. J Jpn Soc Civ Eng Ser B2 Coast Eng 2014;70:471–5. in Japanese.
[71] Lau YL, Moir JR. Booms used for oil slick control. J Environ Eng Div Am Soc Civ Eng 1979;105:369–82. https://doi.org/10.1061/JEEGAV.0000896.
[72] Drysdale D. An introduction to fire dynamics. 3rd edition. Hoboken NJ: Wiley; 2011.
[73] Beyler CL. Fire hazard calculations for large, open hydrocarbon fires. Hurley MJ, Gottuk D, Hall JR, Harada K, Kuligowski E, Puchovsky M, Torero J, Watts JM, Wieczorek C, editors.. SFPE handbook of fire protection engineering. 5th Edition. New York: Springer; 2016. p. 2601–5.
[74] Modak AT. Thermal radiation from pool fires. Combust Flame 1977;29:177–92. https://doi.org/10.1016/0010-2180(77)90106-7.
[75] The Headquarters for Earthquake Research Promotion. Long-term evaluation of earthquakes in the Nankai trough. The Headquarters for Earthquake Research Promotion; 2013 (second edition)Available at, http://www.jishin.go.jp/main/chousa/13may_nankai/index.htm. accessed 6 October 2022.
[76] Central Disaster Management Council. Working group report on megathrust earthquake models for the Nankai Trough, Japan. Cabinet Office of the Japanese Government; 2012. Available at: https://www.bousai.go.jp/jishin/nankai/nankaitrough_info.html. accessed 6 October 2022.
[77] Osaka Prefecture. Disaster prevention plan for petrochemical industrial parks in Osaka. 2022. Available at: https://www.pref.osaka.lg.jp/hoantaisaku/bousaikeikaku/bousaikeikaku2203.html (accessed 6 October 2022).
[78] Blinov V.I., Khudyakov G.N. Diffusion burning of liquids. Izdatel'stvo Akademii Nauk SSSR, Moscow. English Translation, U.S. Army Engineer Research and Development Laboratories, Information Resources Branch, Translation Analysis Section, Fort Belvoir, Virginia, No. T-1490a-C (1961).
[79] Grezio A, Babeyko A, Baptista MA, et al. Probabilistic tsunami hazard analysis: multiple sources and global applications. Rev Geophys 2017;55(4):1158–98. https://doi.org/10.1002/2017RG000579.
[80] Behrens J, Løvholt F, Jalayer F, et al. Probabilistic tsunami hazard and risk analysis: a review of research gaps. Front Earth Sci 2021;9:1–28. https://doi.org/10.3389/feart.2021.628772.
[81] Baba T, Takahashi N, Kaneda Y, Ando K, Matsuoka D, Kato T. Parallel implementation of dispersive tsunami wave modeling with a nesting algorithm for the 2011 Tohoku tsunami. Pure Appl Geophys 2015;172(12):3455–72. https://doi.org/10.1007/s00024-015-1049-2.
[82] Porter K., Byers W., Dykstra D., Lim A., Lynett P., Ratliff J., Scawthorn C., Wein A., Wilson R., 2013, The SAFRR tsunami scenario—physical damage in California, chap. E in Ross SL, and Jones LM, eds., The SAFRR (science application for risk reduction) tsunami scenario: U.S. Geological Survey Open-File Report 2013–1170, 168 p., http://pubs.usgs.gov/of/2013/1170/e/.
[83] Di Maio F, Belotti M, Volpe M, Selva J, Zio E. Parallel density scanned adaptive Kriging to improve local tsunami hazard assessment for coastal infrastructures. Reliab Eng Syst Saf 2022;222:108441. https://doi.org/10.1016/j.ress.2022.108441.